ILoRA: Federated Learning with Low-Rank Adaptation for Heterogeneous Client Aggregation

First Author Junchao Zhou College of Intelligence and Computing, Tianjin University

junchaozhouu@gmail.com

Second Author Institution2

College of Intelligence and Computing, Tianjin University

junkangliukk@gmail.com

Fanhua Shang

School of Computer Science and Technology, Tianjin University, Tianjin, China

fhshang@tju.edu.cn

Abstract

Federated Learning with Low-Rank Adaptation (LoRA) faces three critical challenges under client heterogeneity: (1) Initialization-Induced Instability due to random initialization misaligning client subspaces; (2) Rank Incompatibility and Aggregation Error when averaging LoRA parameters of different ranks, which biases the global model; and (3) exacerbated Client Drift under Non-IID Data, impairing generalization. To address these challenges, we propose ILoRA, a unified framework that integrates three core innovations: a QR-based orthonormal initialization to ensure all clients start in a coherent subspace; a Concatenated OR Aggregation mechanism that fuses heterogeneous-rank updates via concatenation and decomposition, preserving information while maintaining dimension alignment; and an AdamW optimizer with rankaware control variates to correct local updates and mitigate client drift. Supported by theoretical convergence guarantees, extensive experiments on vision and NLP benchmarks demonstrate that ILoRA consistently achieves superior accuracy and convergence stability compared to existing federated LoRA methods.

1. Introduction

The rapid progress of foundation models has significantly advanced AI capabilities in vision and language domains [4, 9, 40]. However, full-parameter fine-tuning of these mod-

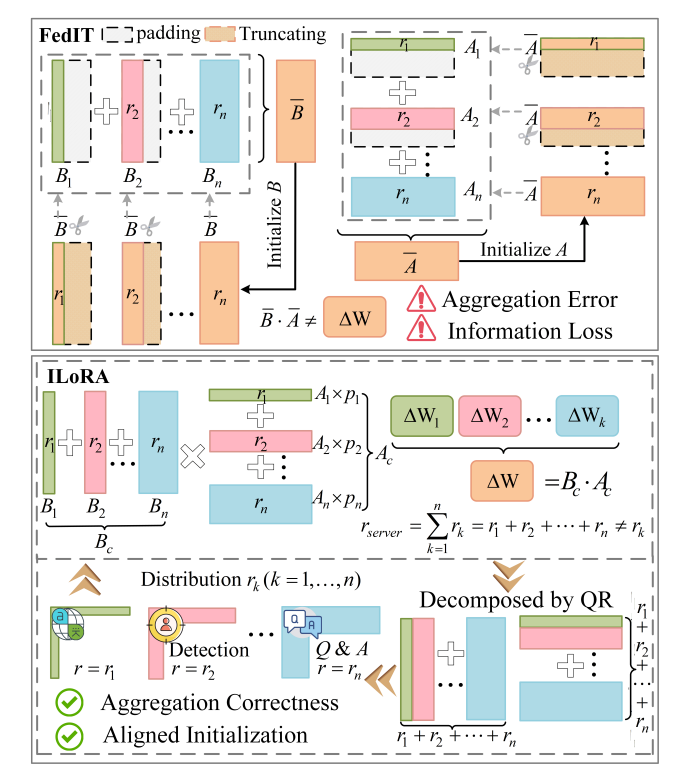


Figure 1. Comparison of federated LoRA methods: **FedIT** (aggregation error and information loss) and **ILoRA** (**ours**) (both correct aggregation and aligned initialization).

els remains computationally expensive and data-intensive [4, 9]. To address this, Parameter-Efficient Fine-Tuning

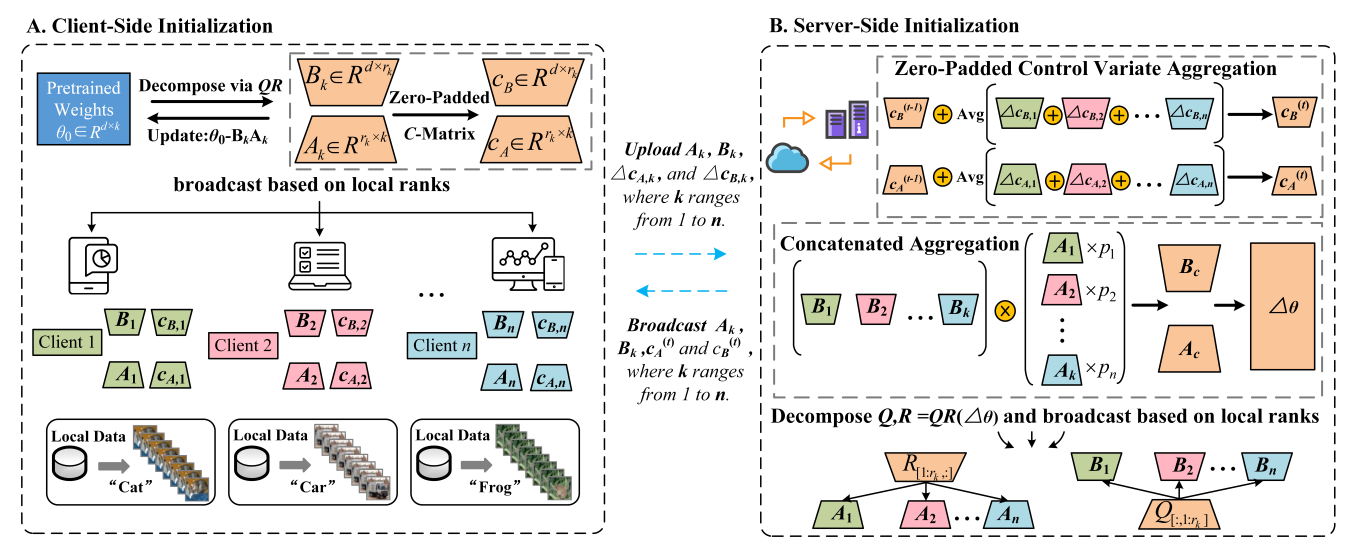


Figure 2. Overview of ILoRA: Clients fine-tune LoRA modules locally; the server aggregates updates via concatenated QR decomposition into a global orthogonal basis (Q, R), enabling efficient communication, subspace alignment, and drift mitigation under Non-IID data.

(PEFT) methods have been developed, which freeze the pre-trained backbone and update only a small set of auxiliary parameters [19, 28, 41, 49]. Among these, LoRA has emerged as a prominent approach, maintaining the base model's representational capacity while enabling efficient adaptation via low-rank update matrices [5, 19, 28, 41].

FL facilitates collaborative model training across decentralized clients without raw data sharing, ensuring privacy-preserving adaptation [6, 14, 20, 32]. Although LoRA integration offers parameter efficiency and privacy in FL, practical systems encounter substantial client heterogeneity in computation, communication, and data distributions. Such heterogeneity induces divergent LoRA ranks and Non-IID data partitions [18, 20, 26, 51], leading to aggregation misalignment, convergence instability, and performance degradation [2, 3, 7, 26, 43, 51].

This paper studies the integration of FL with parameterefficient fine-tuning, focusing on the federated fine-tuning of LoRA. We identify three critical challenges:

Challenge 1: Initialization-Induced Instability. Random initialization of LoRA across clients creates misaligned adaptation subspaces [6], slowing convergence, and destabilizing training [3, 5, 19].

Challenge 2: Rank Incompatibility and Aggregation Error. Heterogeneous client resources lead to varying LoRA ranks [38], yet standard FL aggregation assumes parameter alignment [13], causing aggregation errors and biased global models [2, 7, 43].

Challenge 3: Client Drift under Non-IID Data. LoRA's low-rank parameterization amplifies FL's statistical heterogeneity [15, 25], increasing local-global update divergence. Subspace misalignment further impedes variance reduction, worsening optimization instability [18, 21, 26, 51].

Existing methods for federated fine-tuning fail to address

all three challenges simultaneously in heterogeneous environments. While some target specific issues [1, 8], each has critical limitations: FedIT improves communication but requires homogeneous ranks [48]; FLoRA allows rank heterogeneity but incurs high communication costs and fails to stabilize training [43]; SCAFFOLD reduces Non-IID bias but cannot handle rank variations [21]. Similarly, personalized FL methods using clustering or distillation [33, 46] are incompatible with rank-heterogeneous parameter spaces.

To address these challenges, we propose **ILoRA**, the first framework to systematically apply QR decomposition for federated LoRA fine-tuning. Our unified approach integrates: **QR-based initialization** for subspace alignment [3, 5], **concatenated QR aggregation** for rank-heterogeneous fusion [12, 47, 52], and **AdamW with control variates** for drift mitigation [21]. Supported by theory [34] and extensive experiments [4, 8, 9, 40, 42], ILoRA achieves superior accuracy and stability, as shown in Fig. 1. Our key contributions are summarized as follows:

- The ILoRA Framework. A unified solution addressing initialization instability, rank-heterogeneous aggregation, and client drift in federated LoRA fine-tuning.
- QR-based Heterogeneous Aggregation. A novel protocol fusing different LoRA ranks into a unified subspace via concatenation and QR decomposition.
- Coherent Initialization and Optimization. Orthonormal initialization ensuring subspace consistency, with rank-aware control variates for drift mitigation.
- Theoretical and Empirical Validation. Convergence guarantees and extensive experiments demonstrating state-of-the-art performance.

2. Related Work

Parameter-Efficient Fine-Tuning. PEFT methods adapt large models efficiently by updating minimal parameters while freezing the backbone [13]. Leading approaches include Adapter [17], Prefix-Tuning [27], Prompt Tuning [24], and LoRA [19] with its low-rank decomposition. Recent variants introduce adaptive ranks (AdaLoRA) [49], orthogonal constraints (OLoRA) [5], weight decomposition (DoRA) [28], and dynamic ranks (DyLoRA) [41]. While showing strong centralized performance, these methods remain largely unexplored in federated settings.

Parameter-Efficient Fine-Tuning in FL. Recent works integrate PEFT with FL to reduce communication costs while preserving privacy [10]. FedIT [48] pioneers LoRA for federated instruction tuning, but introduces significant aggregation noise by independently averaging LoRA factors. FLoRA [43] addresses rank heterogeneity via parameter concatenation, yet suffers from $O(K \cdot r_{\rm max})$ communication overhead and dimension mismatch. FFA-LoRA [39] improves stability via partial freezing but lacks proper dimension alignment [38], while LoRA-FAIR [3] enhances aggregation but requires homogeneous ranks.

Heterogeneity in Federated PEFT. A core challenge in federated PEFT is heterogeneity, including both Non-IID data and systemic rank variations. Traditional aggregation methods fail under varying LoRA ranks due to dimension mismatch. Existing solutions have distinct limitations: Zero-padding causes optimization bias under large rank differences [7]; SVD-based methods exhibit error amplification with rank ratios exceeding 2:1 [28]; and Full concatenation incurs high communication overhead [43].

Data Heterogeneity in Federated Learning. Non-IID data induces client drift, degrading accuracy and slowing convergence. Existing mitigation methods include FedProx [26], SCAFFOLD [21], FedCM [44], FedOpt [36], and FedLADA [45]. Personalized FL offers customization but assumes dimension consistency or fails in rank-heterogeneous settings. ILoRA overcomes this via rank-aware control variate AdamW, extending variance reduction to rank-heterogeneous Non-IID environments.

3. Preliminaries

3.1. Federated Learning

Federated Learning (FL) enables collaborative model training across decentralized clients without data sharing [32]. The global objective minimizes:

$$\min_{\boldsymbol{\theta}} F(\boldsymbol{\theta}) = \sum_{k=1}^{K} p_k F_k(\boldsymbol{\theta}), \tag{1}$$

where K is the client count, $p_k = n_k/n$ weights client k with local data size n_k , $n = \sum_{k=1}^K n_k$ is the total data

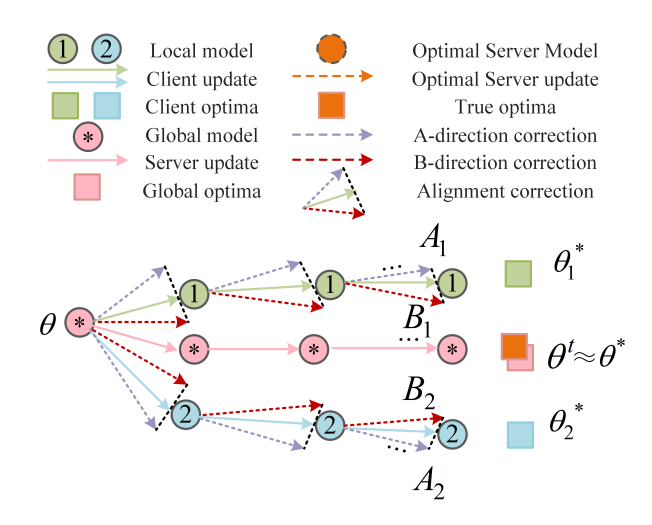


Figure 3. Federated learning model updates with alignment correction. Local models (Client 1 and 2) are guided by corrections, leading the global model to converge near the true optima.

```
Algorithm 1 Client-Side Procedure for two Methods ILoRA and ILoRA-S
```

Input: Local dataset \mathcal{D}_k ; local rank r_k ; local epochs E; learning rate η ; local control variates $\mathbf{c}_{A,k}, \mathbf{c}_{B,k}$.

```
1: if first round then
           Compute QR decomposition: \mathbf{Q}_k, \mathbf{R}_k \leftarrow \mathrm{QR}(\boldsymbol{\theta}_0);
  2:
  3:
           Initialize LoRA: \mathbf{A}_k \leftarrow \mathbf{R}_{k,:r_k,:}, \mathbf{B}_k \leftarrow \mathbf{Q}_{k,:,:r_k};
           Initialize local model: \theta_k \leftarrow \theta_0 - \mathbf{B}_k \mathbf{A}_k;
  4:
  5: else
           Receive \{\mathbf{A}_k, \mathbf{B}_k\}, \ \mathbf{c}_A^{(t-1)}, \mathbf{c}_B^{(t-1)} \ ;
  6:
            Update local model: \theta_k \leftarrow \theta_k + \mathbf{B}_k \mathbf{A}_k;
  7:
      end if
  8:
  9: for e = 1 to E do
           for each mini-batch B in \mathcal{D}_k do
10:
                 Sample B from \mathcal{D}_k;
11:
                  Compute \mathbf{g}_A \leftarrow \nabla \mathcal{L}_k / \partial \mathbf{A}_k, \mathbf{g}_B \leftarrow \nabla \mathcal{L}_k / \partial \mathbf{B}_k;
12:
13:
                  Compute \tilde{\mathbf{g}}_A, \tilde{\mathbf{g}}_B via Eqs.(12) and (13);
                  AdamW(\mathbf{A}_k, \mathbf{B}_k, \mathbf{g}_A, \mathbf{g}_B);
14:
                  AdamW(\mathbf{A}_k, \mathbf{B}_k, \tilde{\mathbf{g}}_A, \tilde{\mathbf{g}}_B);
15:
16:
             Update control variates via (14) and (15);
17:
      end for
        Send (\mathbf{A}_k, \mathbf{B}_k, n_k).
        Send (\mathbf{A}_k, \mathbf{B}_k, n_k, \Delta \mathbf{c}_{A,k}, \Delta \mathbf{c}_{B,k}).
```

size, and $F_k(\theta)$ is the local objective. Non-IID data induces client drift [20], degrading performance. This worsens with communication bottlenecks, system heterogeneity, and training instability in federated fine-tuning.

3.2. PEFT with LoRA

LoRA enables efficient fine-tuning by freezing pre-trained weights and learning low-rank updates to specific matrices in θ [19]. For $\theta_0 \in \mathbb{R}^{d \times k}$, LoRA learns:

$$\theta = \theta_0 + \Delta \theta = \theta_0 + \mathbf{B}\mathbf{A},\tag{2}$$

where $\mathbf{B} \in \mathbb{R}^{d \times r}$, $\mathbf{A} \in \mathbb{R}^{r \times k}$, and $r \ll \min(d, k)$. The layer's forward pass becomes:

$$\mathbf{h} = \boldsymbol{\theta}_0 \mathbf{x} + \mathbf{B} \mathbf{A} \mathbf{x},\tag{3}$$

with input \mathbf{x} and output \mathbf{h} . Standard LoRA initializes \mathbf{A} from Gaussian and \mathbf{B} to zero, scaling to control update size. Recent variants use orthonormal initialization [5] and adaptive strategies [41, 49].

4. Challenges in Federated LoRA

4.1. Challenge 1: Initialization-Induced Instability

Standard LoRA's random Gaussian \mathbf{A} and zero \mathbf{B} initialization [19], while effective centrally, causes *early instability* in federated settings: **Subspace Misalignment:** Random \mathbf{A}_k creates conflicting adaptation directions. **First-Round Amplification:** Aggregating misaligned $\{\mathbf{A}_k, \mathbf{B}_k\}$ distorts global updates and impairs convergence.

4.2. Challenge 2: Rank Incompatibility and Aggregation Error

Client heterogeneity induces varying LoRA ranks r_k [7, 43]. Standard federated averaging assumes homogeneous dimensions, becoming invalid under rank heterogeneity. Direct averaging produces $\Delta \theta' = \bar{\mathbf{B}}\bar{\mathbf{A}}$, differing from correct aggregation:

$$\Delta \boldsymbol{\theta} = \sum_{k} p_{k}(\mathbf{B}_{k} \mathbf{A}_{k}) \neq \bar{\mathbf{B}} \bar{\mathbf{A}}.$$
 (4)

This bias persists even with homogeneous ranks, degrading performance [3, 43].

4.3. Challenge 3: Client Drift under Non-IID Data

Non-IID data [20] exacerbates **client drift** in LoRA finetuning, where local gradients $\nabla F_k(\theta)$ deviate from $\nabla F(\theta)$ and aggregated updates move away from the global optimum. In LoRA, drift amplifies because updates depend on subspace orientations via $\Delta \theta = \mathbf{B} \mathbf{A}$. Under Non-IID data, client subspaces can become nearly orthogonal, increasing local-global misalignment [21]. Table 9 (Appendix A.5) shows performance degrading with heterogeneity (e.g., FedIT drops 19% from $\alpha = 0.8$ to 0.4). Figure 15 (Appendix A.5) visualizes this drift. Our control variates mitigate it, achieving robust convergence (Figure 3).

5. Proposed Method: ILoRA

Algorithm 2 Server-Side Procedure for two Methods ILoRA and ILoRA-S

```
Input: \theta_0, K, p, \{r_k\}, r_s, T, \mathbf{c}_A^{(0)}, \mathbf{c}_R^{(0)} \leftarrow \mathbf{0}
   1: for t = 1 to T do
             Sample S_t \subset \{1, \ldots, K\} with |S_t| = \lfloor pK \rfloor;
             N \leftarrow \sum_{k \in \mathcal{S}_t} n_k;
Receive from k \in \mathcal{S}_t:;
   3:
   4:
                    (\mathbf{A}_k, \mathbf{B}_k, n_k);
   5:
                   (\mathbf{A}_k, \mathbf{B}_k, n_k, \Delta \mathbf{c}_{A,k}, \Delta \mathbf{c}_{B,k});
   6.
             Construct A_c and B_c via (8);
   7:
             Compute \Delta \theta \leftarrow \mathbf{B_c A_c};
   8:
             Compute \mathbf{Q}, \mathbf{R} \leftarrow \mathrm{QR}(\Delta \boldsymbol{\theta});
   9:
             Set \mathbf{B}_s \leftarrow \mathbf{Q}_{:,:r_s}, \mathbf{A}_s \leftarrow \mathbf{R}_{:r_s,:};
 10:
               Update global control variates via (16) and (17);
 11:
             Personalize for each k \in \mathcal{S}_t::
 12:
                  \mathbf{B}_k \leftarrow \mathbf{Q}_{:,:r_k}, \mathbf{A}_k \leftarrow \mathbf{R}_{:r_k,:};
 13:
                    Send \{\mathbf{A}_k, \mathbf{B}_k\}.
 14:
                   Send \{\mathbf{A}_k, \mathbf{B}_k, \mathbf{c}_A^{(t)}, \mathbf{c}_B^{(t)}\}.
 15:
 16: end for
```

5.1. QR-Based Orthogonal Initialization

To address initialization instability, ILoRA employs client-generated orthonormal bases for consistent subspace alignment. Each client k with rank r_k computes local QR decomposition:

$$\mathbf{Q}_k, \mathbf{R}_k = QR(\boldsymbol{\theta}_0), \tag{5}$$

and initializes LoRA parameters as:

$$\mathbf{A}_k = \mathbf{R}_{k,:r_k,:}, \quad \mathbf{B}_k = \mathbf{Q}_{k,:,:r_k}. \tag{6}$$

The local model is then initialized:

$$\boldsymbol{\theta}_k = \boldsymbol{\theta}_0 - \mathbf{B}_k \mathbf{A}_k,\tag{7}$$

ensuring all initial updates $\Delta \theta_k = \mathbf{B}_k \mathbf{A}_k$ are confined to consistent subspaces. After receiving updated \mathbf{B}_k and \mathbf{A}_k , the client updates its model with $\theta_k \leftarrow \theta_k + \mathbf{B}_k \mathbf{A}_k$. This subspace coherence stabilizes federated optimization, reducing variance and client drift (Table 15, Appendix B.2).

5.2. Concatenated QR Aggregation

To address aggregation bias in heterogeneous-rank settings, ILoRA reconstructs the global update before compression. For sampled clients S_t with $p_k = n_k/N$, we vertically concatenate weighted **A** and horizontally **B** matrices:

$$\mathbf{A}_{c} = \begin{bmatrix} p_{1}\mathbf{A}_{1} \\ p_{2}\mathbf{A}_{2} \\ \vdots \\ p_{|\mathcal{S}_{t}|}\mathbf{A}_{|\mathcal{S}_{t}|} \end{bmatrix}, \quad \mathbf{B}_{c} = \begin{bmatrix} \mathbf{B}_{1} & \mathbf{B}_{2} & \cdots & \mathbf{B}_{|\mathcal{S}_{t}|} \end{bmatrix}, \quad (8)$$

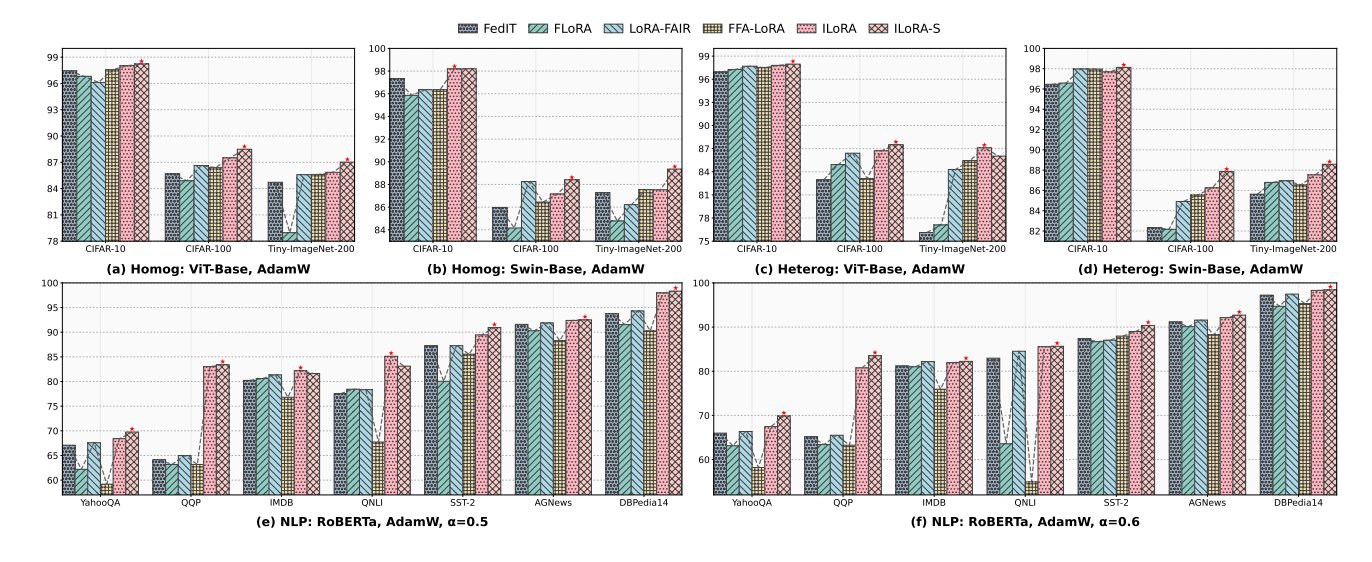


Figure 4. Performance comparison across settings. (a-d) CV tasks with ViT-Base/Swin-Base; (e-f) NLP tasks with RoBERTa.

Table 1. Accuracy comparison (%) of heterogeneous LoRA methods on CIFAR-10/100 and Tiny-ImageNet (ViT/Swin, $Dir(\alpha=0.3)$)

			ViT-	-Base			Swin-Base					
Method	CIFA	AR-10	CIFA	R-100	Tiny-Ir	nageNet	CIFA	AR-10	CIFA	R-100	Tiny-In	nageNet
	SGD	AdamW	SGD	AdamW	SGD	AdamW	SGD	AdamW	SGD	AdamW	SGD	AdamW
FedIT	97.85	97.66	90.09	85.19	87.23	84.72	98.17	97.08	88.30	85.25	87.19	87.40
FLoRA	95.28	97.27	87.66	84.93	83.39	77.10	97.69	96.58	88.75	82.17	88.10	86.79
LoRA-FAIR	97.96	97.69	90.05	86.41	87.41	84.30	97.28	97.97	89.23	84.91	89.13	86.96
FFA-LoRA	97.20	97.50	89.46	83.12	83.90	85.45	97.58	97.96	88.85	85.55	87.28	86.54
ILoRA	98.02	97.80	90.16	86.72	87.29	87.10	98.19	97.69	89.66	86.25	89.44	87.53
ILoRA-S	98.19	97.96	90.39	87.51	87.43	86.03	98.36	98.13	90.51	87.85	89.90	88.58

forming $\Delta \theta = \mathbf{B_c} \mathbf{A_c} = \sum_{k \in \mathcal{S}_t} p_k \mathbf{B}_k \mathbf{A}_k$. Using server rank r_s , we compute QR decomposition:

$$\mathbf{Q}, \mathbf{R} = QR(\Delta \boldsymbol{\theta}) \tag{9}$$

$$\mathbf{B}_s = \mathbf{Q}_{:::r_s}, \quad \mathbf{A}_s = \mathbf{R}_{:r_s::} \tag{10}$$

$$\boldsymbol{\theta}^{(t)} = \boldsymbol{\theta}_0 + \mathbf{B}_s \mathbf{A}_s. \tag{11}$$

Each client receives personalized slices $\mathbf{B}_k = \mathbf{Q}_{:,:r_k}$, $\mathbf{A}_k = \mathbf{R}_{:r_k,:}$, ensuring subspace alignment with $\mathcal{O}(r_s \cdot \max(d,k))$ communication cost.

5.3. AdamW with rank-aware control variates

To mitigate client drift in Non-IID settings, we employ client-specific control variates $\mathbf{c}_{A,k}$ and $\mathbf{c}_{B,k}$ for \mathbf{A}_k and \mathbf{B}_k , initialized to zero. Server $\mathbf{c}_A^{(t-1)}$ and $\mathbf{c}_B^{(t-1)}$ are broadcast each round. Clients compute corrected gradients:

$$\tilde{\mathbf{g}}_{A,k} = \nabla_{\mathbf{A}_k} \mathcal{L}_k + (\mathbf{c}_A^{(t-1)} - \mathbf{c}_{A,k}); \tag{12}$$

$$\tilde{\mathbf{g}}_{B,k} = \nabla_{\mathbf{B}_k} \mathcal{L}_k + (\mathbf{c}_B^{(t-1)} - \mathbf{c}_{B,k}), \tag{13}$$

optimizing A_k and B_k via AdamW. Post-epoch:

$$\Delta \mathbf{c}_{A,k} = \nabla_{\mathbf{A}_k} \mathcal{L}_k - \mathbf{c}_{A,k}, \quad \mathbf{c}_{A,k} \leftarrow \nabla_{\mathbf{A}_k} \mathcal{L}_k; \quad (14)$$

$$\Delta \mathbf{c}_{B,k} = \nabla_{\mathbf{B}_k} \mathcal{L}_k - \mathbf{c}_{B,k}, \quad \mathbf{c}_{B,k} \leftarrow \nabla_{\mathbf{B}_k} \mathcal{L}_k.$$
 (15)

Server aggregates deltas:

$$\mathbf{c}_{A}^{(t)} \leftarrow \mathbf{c}_{A}^{(t-1)} + \frac{1}{|\mathcal{S}_{t}|} \sum_{k \in \mathcal{S}} \Delta \mathbf{c}_{A,k}; \tag{16}$$

$$\mathbf{c}_{B}^{(t)} \leftarrow \mathbf{c}_{B}^{(t-1)} + \frac{1}{|\mathcal{S}_{t}|} \sum_{k \in \mathcal{S}_{t}} \Delta \mathbf{c}_{B,k}. \tag{17}$$

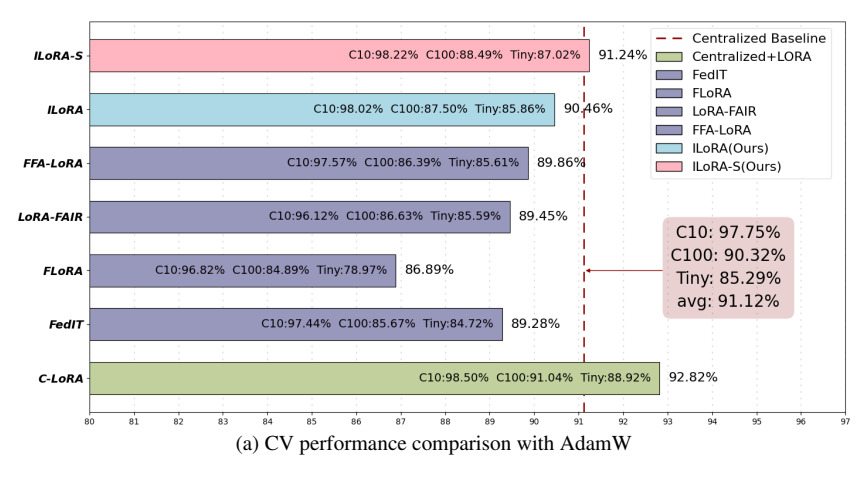
6. Convergence Analysis

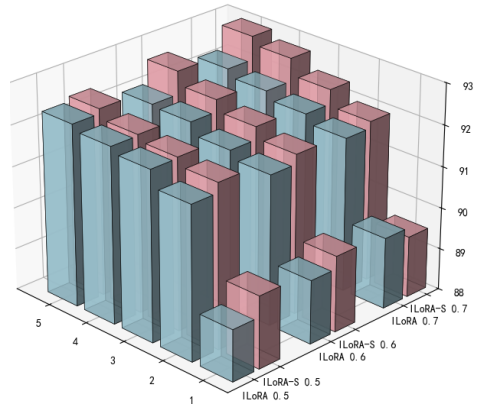
6.1. Theoretical Assumptions

Our analysis relies on the following standard assumptions:

Assumption 1 (L-Smoothness). $\|\nabla F_k(\theta_1) - \nabla F_k(\theta_2)\| \le L\|\theta_1 - \theta_2\|$ holds uniformly across all participating clients.

Assumption 2 (Bounded Gradient Variance). $\mathbb{E}[\|\mathbf{g}_k(\boldsymbol{\theta}) - \nabla F_k(\boldsymbol{\theta})\|^2] \le \sigma^2$ with uniform bound across the federation.





(b) ILoRA vs ILoRA-S with control-based AdamW

Figure 5. Performance comparison under Non-IID settings: (a) Centralized vs. federated learning on CIFAR-10 (C10), CIFAR-100 (C100), and Tiny-ImageNet (Tiny) with $\alpha = 0.3$; (b) AGNews dataset across different heterogeneity levels ($\alpha = 0.5, 0.6, 0.7$).

Table 2. Final accuracy (%) of federated LoRA methods on DomainNet with ViT-Base and Swin-Base after 50 rounds. Best in bold.

					Datasets			
Backbone	Method	Clipart	Infograph	Painting	Quickdraw	Real	Sketch	Average
	FedIT	78.25 base	51.08 _{base}	80.07 base	63.94 _{base}	90.54 _{base}	74.24 _{base}	73.02 _{base}
	FLoRA	$73.80_{_{\downarrow 4.45}}$	$48.34_{\downarrow 2.74}$	$77.52_{\downarrow 2.55}$		$89.55_{\downarrow_{0.99}}$	$68.55_{\downarrow 5.69}$	$68.83_{\downarrow 4.19}$
ViT-Base	LoRA-FAIR	78.49 _{10.24}	51.18 _{↑0.10}	$79.34_{\downarrow 0.73}$	$62.87_{\downarrow 1.07}$	90.56	74.39 _{↑0.15}	$72.81_{\downarrow 0.21}$
VII-Dase	FFA-LoRA	$78.52_{+0.27}$	$49.68_{\downarrow_{1.40}}$	$78.27_{\downarrow_{1.80}}$	63.88	$90.30_{\downarrow_{0.24}}$	$71.37_{\downarrow_{2.87}}$	$72.00_{\downarrow_{1.02}}$
	ILoRA	78.69 _{10.44}	51.44 _{10.36}	80.09	64.18 _{10.24}	90.71	74.78 _{10.54}	73.32
	ILoRA-S	79.83	52.15 _{\(\psi\)1.07}	80.25 _{↑0.18}	65.02 _{↑1.08}	90.96	75.18 _{\(\phi\)0.94}	73.90 _{↑0.88}
	FedIT	86.28 _{base}	61.52 base	84.70 _{base}	73.02 _{base}	92.64 _{base}	84.41 _{base}	80.43 base
	FLoRA	85.58 40.70	58.16	84.54	$70.42_{+2.60}$	$92.11_{\downarrow 0.53}$	81.25	78.68
Swin-Base	LoRA-FAIR	86.85	61.89 _{↑0.37}	84.17 10.53	$72.66_{\downarrow 0.36}$	$92.07_{+0.57}$	84.75	80.40 \(_{\pu0.03}\)
Swiii-Dase	FFA-LoRA	87.19 _{↑0.91}	$61.29_{\downarrow 0.23}$	84.05	$71.71_{\perp_{1.31}}$	91.88 10.76	84.04 10.37	80.03 10.40
	ILoRA	87.32 _{↑1.04}	$61.14_{\pm 0.38}$	85.10 _{10.40}	$73.38_{+0.36}$	92.70	84.90	80.76
	ILoRA-S	88.46 _{↑2.18}	62.11 $_{\uparrow 0.59}$	86.13 _{↑1.43}	75.39 _{↑2.37}	92.75	85.87 _{↑1.46}	81.79 _{↑1.36}

Assumption 3 (Bounded Gradient Heterogeneity). $\|\nabla F_k(\theta) - \nabla F(\theta)\| \le \delta$ quantifying the degree of data heterogeneity among clients in the federated network.

Assumption 4 (Subspace Consistency). $S_k \subseteq S_s = colspan(\mathbf{Q}_{[:,1:r_s]})$ ensuring aligned parameter spaces.

6.2. Main Convergence Results

Theorem 1 (Convergence of ILoRA). *Under Assumptions* 1–4, with $\eta_l \leq 1/L$ and $\eta_q \eta_l = \Theta(1/\sqrt{SKT})$:

$$\frac{1}{T} \sum_{t=1}^{T} \mathbb{E}\left[\|\nabla F(\boldsymbol{\theta}_t)\|^2 \right] \le \mathcal{O}\left(\frac{1}{\sqrt{SKT}} + \frac{\delta^2 + \epsilon_r}{T}\right), \quad (18)$$

where $\epsilon_r = (r_{\text{max}} - r_s)^2$, S: clients/round, K: local steps, T: total rounds.

Proof Sketch. The proof uses QR-based low-rank reconstruction, subspace alignment through orthogonal initialization, and control variates to mitigate client drift, ensuring stability. Details are in Appendix B.1. □

Theorem 2 (Subspace Preservation under QR Compression). For $r_k \leq r_s$, $\mathbf{B}_{r_k} = \mathbf{Q}_{:,:r_k}$ and $\mathbf{A}_{r_k} = \mathbf{R}_{:r_k,:}$ satisfy $\operatorname{colspan}(\mathbf{B}_{r_k}) \subseteq \operatorname{colspan}(\mathbf{Q})$.

Theorem 3 (Consistent Subspace Initialization). $\mathbf{B}_{k}^{(0)} = \mathbf{Q}_{:,:r_{k}}$ and $\mathbf{A}_{k}^{(0)} = \mathbf{R}_{:r_{k},:}$ ensure all clients start in colspan(\mathbf{Q}), reducing gradient variance by $\mathcal{O}(1/K)$.

Theorem 4 (Convergence with Control Variates and AdamW). *Under Assumptions 1–4, with control variates reducing variance to* $\sigma^2(1-\rho^2)$:

$$\frac{1}{T} \sum_{t=1}^{T} \mathbb{E}\left[\|\nabla F(\boldsymbol{\theta}_t)\|^2 \right] \le \mathcal{O}\left(\frac{1}{\sqrt{SKT}} + \frac{\delta^2 + \epsilon_r'}{T}\right), \quad (19)$$

where $\epsilon_r' = (r_s - \bar{r})^2 / r_s^2$, \bar{r} : mean client rank.

Proof Sketch. The proof shows that control variates reduce client drift by correcting gradients $\tilde{\mathbf{g}}_k = \mathbf{g}_k + (\mathbf{c} - \mathbf{c}_k)$, improving convergence. Details are in Appendix B.4.

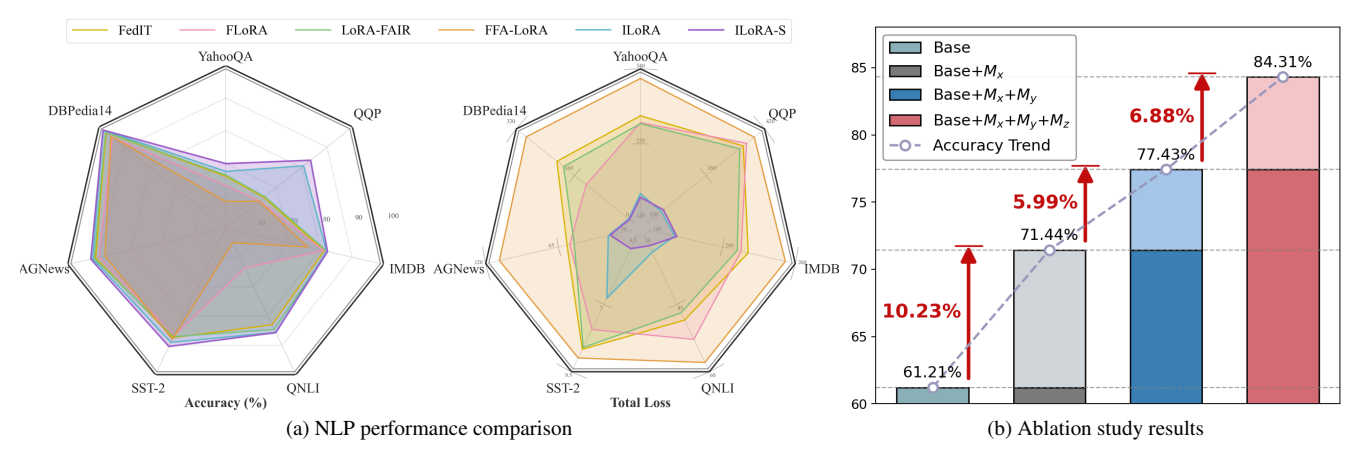


Figure 6. (a) NLP accuracy on datasets with RoBERTa under $Dir(\alpha=0.6)$. (b) Ablation: gains from ILoRA components M_x , M_y , M_z .

Table 3. Peak accuracy comparison (%) of federated heterogeneous LoRA methods on NLP datasets (RoBERTa, Dir(α =0.6)).

Method		NLP Datasets (RoBERTa, Accuracy ↑)									
1,1011104	YahooQA	QQP	IMDB	QNLI	SST-2	AGNews	DBPedia14	Avg.			
FedIT	65.99 _{base}	65.20 _{base}	81.19 hase	82.96 _{base}	87.39 _{base}	91.18 _{base}	97.23 _{base}	81.59 hase			
FLoRA	$63.13_{\downarrow 2.86}$	$63.40_{\downarrow_{1.80}}$	81.01 10.18	$63.57_{\downarrow_{19.39}}$	86.70 10.69	90.09		77.52			
LoRA-FAIR	66.36	65.51	82.19 _{↑1.00}	84.53	87.04 10.35	91.59	97.46	82.10			
FFA-LoRA	58.21	63.26	$75.94_{\downarrow 5.25}$	54.95	87.96	88.21	95.32	74.84			
ILoRA	67.47	80.75	81.96	85.56	88.99	92.14		85.02			
ILoRA-S	69.87 _{↑3.88}	83.52 _{18.32}	82.24	85.65 _{↑2.69}	90.37			86.11			

ILoRA provides strong theoretical guarantees addressing three core federated LoRA challenges: **rank robustness** via QR aggregation (Theorem 6, Appendix B.2), **Non-IID resilience** through control variates (Theorem 10, Appendix B.4), and **communication efficiency** with $\mathcal{O}(r_s \cdot \max(d,k))$ cost (Theorem 13, Appendix B.5).

Theoretical analysis demonstrates $\mathcal{O}(1/\sqrt{SKT})$ convergence (Theorems 5, 10, Appendix B.1, B.4) with bounded heterogeneity effects, global stability (Theorem 16, Appendix B.5), and $\mathcal{O}(1/K)$ variance reduction via orthogonal initialization (Theorem 7, Lemma 4, Appendix B.3). Rank-aware control variates (Lemmas 8, 9, Theorem 11, Appendix B.4) ensure robustness to data and rank heterogeneity. Empirical validation (Tables 15, 14, 18, 16, 17, Appendix B.3, B.2, B.5, B.4) confirms **ILoRA**'s balanced performance across drift mitigation, efficiency, and accuracy.

6.3. Experimental Setup

Models and Datasets. ILoRA is evaluated on CV (ViT-Base [11], Swin-Base [30]) and NLP (RoBERTa [29]) benchmarks. CV datasets: CIFAR-10/100 [22], Tiny-ImageNet [16], DomainNet [35]. NLP: YahooQA [23], QQP, QNLI [42], IMDB [31], SST-2 [37], AGNews and DBPedia14 [50]. All use Non-IID Dirichlet partitioning.

Baselines and Settings. Compared methods: FedIT

[26], FLoRA [43], LoRA-FAIR [3], FFA-LoRA [39]. Unified LoRA configurations and optimization protocols are used across all experiments.

Additional implementation details including hyperparameter settings, hardware configurations, and computational resources are provided in Appendix A.

6.4. Experiment Results

CV Performance under Heterogeneous Settings. ILoRA-S reaches 87.51% on CIFAR-100 with ViT-Base+AdamW (Table 1), improving over LoRA-FAIR by 1.10% and FedIT by 2.32%. It also performs well with Swin-Base (Figure 4(d)), showing heterogeneity resilience. On DomainNet (50 rounds, Table 2), ILoRA-S attains averages of 73.90% (ViT-Base) and 81.79% (Swin-Base), supporting generalization across domains. Performance curves (Figure 4(a,c)) show higher accuracy, supporting subspace alignment and reduced drift. Advantages persist in homogeneous settings (Table 10) and with SGD (Appendix Figures 11-14).

NLP Performance under Heterogeneous Settings. With heterogeneous LoRA ranks and Non-IID data (Dir(α =0.6)), ILoRA achieves 85.02% accuracy on seven NLP benchmarks (Table 3), with ILoRA-S reaching 86.11% and outperforming all baselines (Figure 4). ILoRA-S sets SOTA on six of seven datasets, with large gains on QQP (83.52%, +18.32%), YahooQA (69.87%, +3.88%), and DB-

Table 4. Peak accuracy comparison (%) under different federation scales ($\alpha = 0.5$). "Setting" denotes client count and participation rate

Method	Setting			Datase	ets (Accuracy	<i>'</i> ↑)			Avg.
1,1001100	Setting	YahooQA	QQP	IMDB	QNLI	SST-2	AGNews	DBPedia14	12, 8 ,
FedIT+QF	R 3 (100%)	40.73 _{base}	63.18 _{base}	58.09 hase	64.43 hase	71.90 hase	87.04 _{base}	74.31 _{base}	65.67 _{base}
ILoRA	3 (100%)	63.76 _{↑23.0}	63.66 _{10.5}	78.26 _{↑20.2}	83.51 _{19.1}	82.57 _{10.7}	91.68	97.62 _{↑23.3}	80.15
FedIT+QF	R 15 (80%)	31.88 _{base}	63.18 base	74.78 base	50.58 base	89.79 base	63.11 base	77.39 base	64.39 base
ILoRA	15 (80%)	65.70 _{↑33.8}	77.58 _{14.4}	76.88 _{↑2.1}	62.11 _{11.5}	89.79 _{10.0}	88.17	94.66 _{17.3}	79.27 14.9

Table 5. Peak accuracy comparison (%) under extreme settings (Dir(α =0.1/0.5/1.0), ranks = 2/8/16).

Method	$Dir(\alpha)$			Datase	ets (Accuracy	· †)			Avg.
	()	YahooQA	QQP	IMDB	QNLI	SST-2	AGNews	DBPedia14	
FedIT+QR	0.1	34.07 _{base}	85.36 _{base}	52.40 base	50.54 base	50.92 base	70.75 base	44.06 base	55.44 _{base}
ILoRA	0.1	51.05 _{↑17.0}	84.22	50.14 _{1.2.3}	50.54 _{10.0}	54.82 _{↑3.9}	80.75 _{↑10.0}	87.64 _{143.6}	65.59 _{10.2}
FedIT+QR	0.5	40.73 base	63.18 base	58.09 base	64.43 base	71.90 base	87.04 base	74.31 base	65.67 base
ILoRA	0.5	63.76 _{↑23.0}	63.66	78.26 _{↑20.2}	83.51	82.57 _{10.7}	91.68	97.62 _{123.3}	80.15
FedIT+QR	1.0	60.98 _{base}	63.23 base	81.28 base	50.65 base	55.62 base	80.92 base	75.38 base	66.87 base
ILoRA	1.0	$\textbf{70.90}_{~\uparrow 9.9}$	64.31 _{↑1.1}	81.73 _{10.5}	82.59 _{↑31.9}	88.88	90.57	97.19 _{↑21.8}	82.31 _{15.4}

Table 6. Control variates mitigate client drift on Tiny-ImageNet; ILoRA-S outperforms ILoRA. **Bold** indicates best performance.

Method	$\alpha = 0.5$	$\alpha = 0.6$	$\alpha = 0.7$
ILoRA	$85.14_{\pm0.34}$	$85.90_{\pm 0.51}$	$85.93_{\pm 0.20}$
ILoRA-S	$86.03_{\pm0.32}$	$86.29_{\pm 0.19}$	$86.43_{\pm 0.17}$

Pedia14 (98.43%, +1.20%), visualized in Fig. 7. Consistent superiority at $\alpha=0.5$ (Table 8, Appendix B) confirms robustness. ILoRA variants show better stability, reducing loss 40–95% versus FedIT (Figure 6a) and validating generalization (Figs. 9 and 10, Appendix A.5).

Comparison with Centralized Learning. ILoRA-S achieves the closest performance to centralized training among federated methods under AdamW (Figure 5a), recovering over 95% of centralized accuracy on Tiny-ImageNet and significantly narrowing the performance gap. Similar SGD trends (Appendix A.5, Figure 8) confirm consistent high recovery rates across datasets and optimizers.

6.5. Communication Efficiency Analysis

ILoRA delivers communication efficiency, with downlink $\mathcal{O}(r_s(d+k))$ and uplink $\mathcal{O}(S\cdot r_{\max}(d+k))$ —below FLoRA's $\mathcal{O}(r_{\text{total}}(d+k))$ (Table 17, Appendix B.5). It shows near-constant overhead $(1.2\times-1.6\times$ for 10–100 clients) versus FLoRA's linear rise $(2.5\times-25.0\times)$ (Table 7, Appendix A.5). This $\mathcal{O}(1)$ scaling via QR compression makes ILoRA suited for large-scale federated deployments.

6.6. Ablation Study

Effectiveness of Server-Side Aggregation. Our concatenated QR aggregation outperforms FedIT+QR across set-

tings: Table 11 in Appendix A.5 shows 9.08% improvement at high heterogeneity ($\alpha=0.7$); Table 5 demonstrates robustness under extreme heterogeneity ($\alpha=0.1,0.5,1.0$) and diverse ranks (2,8,16) with 10.15–15.44% gains; Table 4 confirms scalability to 15-client settings (14.88% improvement) comparable to 3-client performance (14.48%). These results validate generalization across heterogeneity levels, parameter configurations, and federation scales.

Client Drift Suppression via AdamW Optimization ILoRA-S mitigates client drift on CV and NLP. On CIFAR-100, it reaches 89.00% accuracy with std 0.07-0.33 across $\alpha = 0.5-0.7$ (Table 13, Appendix A.5). On Tiny-ImageNet, it maintains 0.9-1.0% gains over ILoRA (Table 6). For NLP, ILoRA-S improves AGNews (Table 12, Appendix A.5) to 92.87% at $\alpha = 0.7$ and outperforms ILoRA across heterogeneity levels. These results demonstrate the effectiveness of our control variate mechanism in suppressing client drift in heterogeneous federated settings. **Cumulative Benefits of Component Integration** Ablation studies on QNLI (Figure 6b) show complementary gains from ILoRA's core components: orthogonal initialization (M_x) aligns subspaces, concatenated aggregation (M_y) enables cross-client fusion, and control variates (M_z) suppress drift. Cumulative improvements validate our holistic design where each mechanism addresses distinct federated LoRA challenges while synergistically enhancing performance.

7. Conclusion

In this work, we proposed **ILoRA** to address the key challenges of initialization instability, rank-incompatible aggregation, and client drift in federated LoRA finetuning. Our unified framework systematically integrates

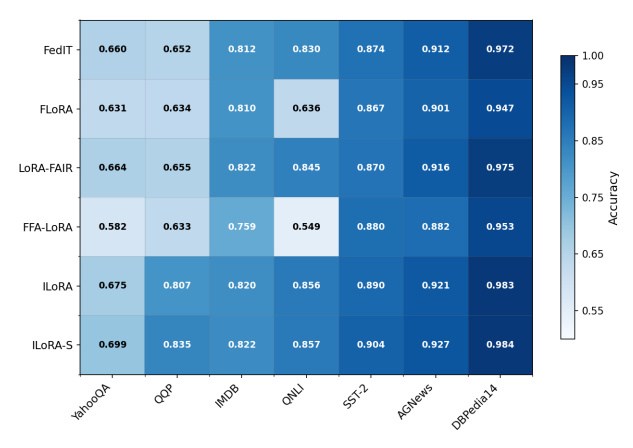


Figure 7. NLP accuracy heatmap (RoBERTa, Dir(α =0.6))

three core innovations: QR-based orthogonal initialization for stable subspace alignment, concatenated QR aggregation for exact heterogeneous-rank fusion, and rank-aware control variates for effective drift mitigation. Supported by theoretical convergence guarantees and extensive experiments across diverse vision and NLP benchmarks, ILoRA consistently achieves state-of-the-art performance while maintaining communication efficiency. This work establishes a principled foundation for federated fine-tuning under heterogeneity, with future extensions planned for broader parameter-efficient methods and more constrained federated environments.

References

- [1] Sara Babakniya, Ahmed Roushdy Elkordy, Yahya H Ezzeldin, Qingfeng Liu, Kee-Bong Song, Mostafa El-Khamy, and Salman Avestimehr. Slora: Federated parameter efficient fine-tuning of language models. *arXiv preprint* arXiv:2308.06522, 2023. 2
- [2] Jiamu Bai, Daoyuan Chen, Bingchen Qian, Liuyi Yao, and Yaliang Li. Federated fine-tuning of large language models under heterogeneous tasks and client resources. *Advances in Neural Information Processing Systems*, 37:14457–14483, 2024. 2
- [3] Jieming Bian, Lei Wang, Letian Zhang, and Jie Xu. Lorafair: Federated lora fine-tuning with aggregation and initialization refinement. *arXiv preprint arXiv:2411.14961*, 2024. 2, 3, 4, 7, 1
- [4] Tom Brown, Benjamin Mann, Nick Ryder, Melanie Subbiah, Jared D Kaplan, Prafulla Dhariwal, Arvind Neelakantan, Pranav Shyam, Girish Sastry, Amanda Askell, et al. Language models are few-shot learners. Advances in neural information processing systems, 33:1877–1901, 2020. 1, 2
- [5] Kerim Büyükakyüz. Olora: Orthonormal low-rank adaptation of large language models. *arXiv preprint arXiv:2406.01775*, 2024. 2, 3, 4
- [6] Sebastian Caldas, Sai Meher Karthik Duddu, Peter Wu, Tian Li, Jakub Konečný, H Brendan McMahan, Virginia Smith, and Ameet Talwalkar. Leaf: A benchmark for federated settings. arXiv preprint arXiv:1812.01097, 2018. 2

- [7] Yae Jee Cho, Luyang Liu, Zheng Xu, Aldi Fahrezi, and Gauri Joshi. Heterogeneous lora for federated fine-tuning of on-device foundation models. arXiv preprint arXiv:2401.06432, 2024. 2, 3, 4, 1
- [8] Jia Deng, Wei Dong, Richard Socher, Li-Jia Li, Kai Li, and Li Fei-Fei. Imagenet: A large-scale hierarchical image database. In 2009 IEEE conference on computer vision and pattern recognition, pages 248–255. Ieee, 2009. 2
- [9] Jacob Devlin, Ming-Wei Chang, Kenton Lee, and Kristina Toutanova. Bert: Pre-training of deep bidirectional transformers for language understanding. In Proceedings of the 2019 conference of the North American chapter of the association for computational linguistics: human language technologies, volume 1 (long and short papers), pages 4171–4186, 2019. 1, 2
- [10] Ning Ding, Yujia Qin, Guang Yang, Fuchao Wei, Zonghan Yang, Yusheng Su, Shengding Hu, Yulin Chen, Chi-Min Chan, Weize Chen, et al. Parameter-efficient fine-tuning of large-scale pre-trained language models. *Nature Machine Intelligence*, 5(3):220–235, 2023.
- [11] Alexey Dosovitskiy. An image is worth 16x16 words: Transformers for image recognition at scale. arXiv preprint arXiv:2010.11929, 2020. 7
- [12] GH Golub and CF Van Loan. Matrix computations 4th edition the johns hopkins university press. *Baltimore*, MD, 2013. 2
- [13] Zeyu Han, Chao Gao, Jinyang Liu, Jeff Zhang, and Sai Qian Zhang. Parameter-efficient fine-tuning for large models: A comprehensive survey. arXiv preprint arXiv:2403.14608, 2024. 2, 3
- [14] Andrew Hard, Kanishka Rao, Rajiv Mathews, Swaroop Ramaswamy, Françoise Beaufays, Sean Augenstein, Hubert Eichner, Chloé Kiddon, and Daniel Ramage. Federated learning for mobile keyboard prediction. arXiv preprint arXiv:1811.03604, 2018. 2
- [15] Junxian He, Chunting Zhou, Xuezhe Ma, Taylor Berg-Kirkpatrick, and Graham Neubig. Towards a unified view of parameter-efficient transfer learning. arXiv preprint arXiv:2110.04366, 2021. 2
- [16] Dan Hendrycks and Thomas Dietterich. Benchmarking neural network robustness to common corruptions and perturbations. arXiv preprint arXiv:1903.12261, 2019. 7
- [17] Neil Houlsby, Andrei Giurgiu, Stanislaw Jastrzebski, Bruna Morrone, Quentin De Laroussilhe, Andrea Gesmundo, Mona Attariyan, and Sylvain Gelly. Parameter-efficient transfer learning for nlp. In *International conference on machine learning*, pages 2790–2799. PMLR, 2019. 3
- [18] Tzu-Ming Harry Hsu, Hang Qi, and Matthew Brown. Measuring the effects of non-identical data distribution for federated visual classification. arXiv preprint arXiv:1909.06335, 2019.
- [19] Edward J Hu, Yelong Shen, Phillip Wallis, Zeyuan Allen-Zhu, Yuanzhi Li, Shean Wang, Lu Wang, Weizhu Chen, et al. Lora: Low-rank adaptation of large language models. *ICLR*, 1(2):3, 2022. 2, 3, 4
- [20] Peter Kairouz, H Brendan McMahan, Brendan Avent, Aurélien Bellet, Mehdi Bennis, Arjun Nitin Bhagoji, Kallista

- Bonawitz, Zachary Charles, Graham Cormode, Rachel Cummings, et al. Advances and open problems in federated learning. *Foundations and trends*® *in machine learning*, 14(1–2): 1–210, 2021. 2, 3, 4
- [21] Sai Praneeth Karimireddy, Satyen Kale, Mehryar Mohri, Sashank Reddi, Sebastian Stich, and Ananda Theertha Suresh. Scaffold: Stochastic controlled averaging for federated learning. In *International conference on machine learn*ing, pages 5132–5143. PMLR, 2020. 2, 3, 4
- [22] Alex Krizhevsky, Geoffrey Hinton, et al. Learning multiple layers of features from tiny images.(2009), 2009. 7
- [23] Onur Kucuktunc, B Barla Cambazoglu, Ingmar Weber, and Hakan Ferhatosmanoglu. A large-scale sentiment analysis for yahoo! answers. In *Proceedings of the fifth ACM international conference on Web search and data mining*, pages 633–642, 2012. 7
- [24] Brian Lester, Rami Al-Rfou, and Noah Constant. The power of scale for parameter-efficient prompt tuning. *arXiv* preprint *arXiv*:2104.08691, 2021. 3
- [25] Qinbin Li, Yiqun Diao, Quan Chen, and Bingsheng He. Federated learning on non-iid data silos: An experimental study. In 2022 IEEE 38th international conference on data engineering (ICDE), pages 965–978. IEEE, 2022. 2
- [26] Tian Li, Anit Kumar Sahu, Manzil Zaheer, Maziar Sanjabi, Ameet Talwalkar, and Virginia Smith. Federated optimization in heterogeneous networks. *Proceedings of Machine learning and systems*, 2:429–450, 2020. 2, 3, 7
- [27] Xiang Lisa Li and Percy Liang. Prefix-tuning: Optimizing continuous prompts for generation. *arXiv preprint arXiv:2101.00190*, 2021. 3
- [28] Shih-Yang Liu, Chien-Yi Wang, Hongxu Yin, Pavlo Molchanov, Yu-Chiang Frank Wang, Kwang-Ting Cheng, and Min-Hung Chen. Dora: Weight-decomposed low-rank adaptation. In Forty-first International Conference on Machine Learning, 2024. 2, 3
- [29] Yinhan Liu, Myle Ott, Naman Goyal, Jingfei Du, Mandar Joshi, Danqi Chen, Omer Levy, Mike Lewis, Luke Zettlemoyer, and Veselin Stoyanov. Roberta: A robustly optimized bert pretraining approach. arXiv preprint arXiv:1907.11692, 2019. 7
- [30] Ze Liu, Yutong Lin, Yue Cao, Han Hu, Yixuan Wei, Zheng Zhang, Stephen Lin, and Baining Guo. Swin transformer: Hierarchical vision transformer using shifted windows. In *Proceedings of the IEEE/CVF international conference on computer vision*, pages 10012–10022, 2021. 7
- [31] Andrew Maas, Raymond E Daly, Peter T Pham, Dan Huang, Andrew Y Ng, and Christopher Potts. Learning word vectors for sentiment analysis. In *Proceedings of the 49th an*nual meeting of the association for computational linguistics: Human language technologies, pages 142–150, 2011.
- [32] Brendan McMahan, Eider Moore, Daniel Ramage, Seth Hampson, and Blaise Aguera y Arcas. Communication-efficient learning of deep networks from decentralized data. In *Artificial intelligence and statistics*, pages 1273–1282. PMLR, 2017. 2, 3
- [33] Mahdi Morafah, Saeed Vahidian, Weijia Wang, and Bill Lin. Flis: Clustered federated learning via inference similarity for

- non-iid data distribution. *IEEE Open Journal of the Computer Society*, 4:109–120, 2023. 2
- [34] Behnam Neyshabur, Srinadh Bhojanapalli, David McAllester, and Nathan Srebro. A theoretical framework for understanding the generalization of deep learning models. In Advances in Neural Information Processing Systems, 2017. 2
- [35] Xingchao Peng, Qinxun Bai, Xide Xia, Zijun Huang, Kate Saenko, and Bo Wang. Moment matching for multi-source domain adaptation. In *Proceedings of the IEEE/CVF inter*national conference on computer vision, pages 1406–1415, 2019. 7
- [36] Sashank Reddi, Zachary Charles, Manzil Zaheer, Zachary Garrett, Keith Rush, Jakub Konečný, Sanjiv Kumar, and H Brendan McMahan. Adaptive federated optimization. arXiv preprint arXiv:2003.00295, 2020. 3
- [37] Richard Socher, Alex Perelygin, Jean Wu, Jason Chuang, Christopher D Manning, Andrew Y Ng, and Christopher Potts. Recursive deep models for semantic compositionality over a sentiment treebank. In *Proceedings of the 2013* conference on empirical methods in natural language processing, pages 1631–1642, 2013. 7
- [38] Shangchao Su, Bin Li, and Xiangyang Xue. Fedra: A random allocation strategy for federated tuning to unleash the power of heterogeneous clients. *arXiv preprint* arXiv:2311.11227, 2023. 2, 3
- [39] Youbang Sun, Zitao Li, Yaliang Li, and Bolin Ding. Improving lora in privacy-preserving federated learning. *arXiv* preprint arXiv:2403.12313, 2024. 3, 7, 1
- [40] Hugo Touvron, Thibaut Lavril, Gautier Izacard, Xavier Martinet, Marie-Anne Lachaux, Timothée Lacroix, Baptiste Rozière, Naman Goyal, Eric Hambro, Faisal Azhar, et al. Llama: Open and efficient foundation language models. arXiv preprint arXiv:2302.13971, 2023. 1, 2
- [41] Mojtaba Valipour, Mehdi Rezagholizadeh, Ivan Kobyzev, and Ali Ghodsi. Dylora: Parameter efficient tuning of pretrained models using dynamic search-free low-rank adaptation. *arXiv preprint arXiv:2210.07558*, 2022. 2, 3, 4
- [42] Alex Wang, Amanpreet Singh, Julian Michael, Felix Hill, Omer Levy, and Samuel R Bowman. Glue: A multi-task benchmark and analysis platform for natural language understanding. arXiv preprint arXiv:1804.07461, 2018. 2, 7
- [43] Ziyao Wang, Zheyu Shen, Yexiao He, Guoheng Sun, Hongyi Wang, Lingjuan Lyu, and Ang Li. Flora: Federated finetuning large language models with heterogeneous low-rank adaptations. *Advances in Neural Information Processing Systems*, 37:22513–22533, 2024. 2, 3, 4, 7, 1
- [44] Jing Xu, Sen Wang, Liwei Wang, and Andrew Chi-Chih Yao. Fedem: Federated learning with client-level momentum. *arXiv preprint arXiv:2106.10874*, 2021. 3
- [45] Yunfei Yang and Ding-Xuan Zhou. Nonparametric regression using over-parameterized shallow relu neural networks. *Journal of Machine Learning Research*, 25(165):1–35, 2024.
- [46] Zhiqin Yang, Yonggang Zhang, Yu Zheng, Xinmei Tian, Hao Peng, Tongliang Liu, and Bo Han. Fedfed: Feature distillation against data heterogeneity in federated learning. Ad-

- vances in Neural Information Processing Systems, 36, 2024.
- [47] Elad Ben Zaken, Shauli Ravfogel, and Yoav Goldberg. Bitfit: Simple parameter-efficient fine-tuning for transformer-based masked language-models. *arXiv preprint arXiv:2106.10199*, 2021. 2
- [48] Jianyi Zhang, Saeed Vahidian, Martin Kuo, Chunyuan Li, Ruiyi Zhang, Tong Yu, Guoyin Wang, and Yiran Chen. Towards building the federatedgpt: Federated instruction tuning. In ICASSP 2024-2024 IEEE International Conference on Acoustics, Speech and Signal Processing (ICASSP), pages 6915–6919. IEEE, 2024. 2, 3, 1
- [49] Qingru Zhang, Minshuo Chen, Alexander Bukharin, Nikos Karampatziakis, Pengcheng He, Yu Cheng, Weizhu Chen, and Tuo Zhao. Adalora: Adaptive budget allocation for parameter-efficient fine-tuning. *arXiv preprint arXiv:2303.10512*, 2023. 2, 3, 4
- [50] Xiang Zhang, Junbo Zhao, and Yann LeCun. Character-level convolutional networks for text classification. *Advances in neural information processing systems*, 28, 2015. 7
- [51] Yue Zhao, Meng Li, Liangzhen Lai, Naveen Suda, Damon Civin, and Vikas Chandra. Federated learning with non-iid data. arXiv preprint arXiv:1806.00582, 2018. 2
- [52] Jiacheng Zhu, Kristjan Greenewald, Kimia Nadjahi, Haitz Sáez de Ocáriz Borde, Rickard Brüel Gabrielsson, Leshem Choshen, Marzyeh Ghassemi, Mikhail Yurochkin, and Justin Solomon. Asymmetry in low-rank adapters of foundation models. arXiv preprint arXiv:2402.16842, 2024. 2

ILoRA: Federated Learning with Low-Rank Adaptation for Heterogeneous Client Aggregation

Supplementary Material

A. Implementation and Experimental Setup Details

A.1. Models and Tasks

We conduct experiments on standard benchmarks in both Computer Vision (CV) and Natural Language Processing (NLP). For CV tasks, we adopt two widely-used Transformer-based architectures: *VIT-Base* (Vision Transformer) and *Swin-Base* (Swin Transformer). In the NLP domain, we utilize *RoBERTa* for text classification and textual entailment tasks. All models are fine-tuned in a federated learning scenario with parameter-efficient *LoRA* adapters.

Our experimental evaluation encompasses standard benchmarks in both computer vision (CV) and natural language processing (NLP). For CV tasks, we employ two prominent Transformer-based architectures: *ViT-Base* (86M parameters) and *Swin-Base* (88M parameters), fine-tuned for image classification. In the NLP domain, we utilize *RoBERTa* (125M parameters) for a diverse set of tasks including text classification, natural language inference, and question-answering. All models are fine-tuned within a federated learning framework using parameter-efficient *LoRA* adapters, ensuring a consistent and comparable experimental setup across all domains and baselines.

A.2. Baselines

We compare **ILoRA** with four state-of-the-art federated LoRA baselines:

- **FedIT** [48]: a federated instruction-tuning approach that adopts *homogeneous* LoRA ranks.
- **FLoRA** [43]: enables *heterogeneous* LoRA ranks via parameter concatenating[7].
- LoRA-FAIR [3]: refines aggregation and initialization under homogeneous ranks.
- **FFA-LoRA** [39]: improves training stability by freezing a subset of adapter parameters.
- ILoRA: our proposed method.
- ILoRA-S: an extended variant that incorporates rankaware control variates.

For a fair comparison, all baselines are implemented under the identical LoRA configuration.

A.3. Hyperparameter Settings

We adopt a unified configuration across all experiments. LoRA is applied to the self-attention *query* and *value* projections, with the client-side rank fixed at 4. On the server, we use rank 4 in homogeneous settings and rank 6 in hetero-

geneous settings; FLoRA uses rank 12 in both cases. The LoRA scaling factor is 16, with a dropout rate of 0.1 and a global scaling factor of 0.5. For optimization, we compare stochastic gradient descent (learning rate 0.01, momentum 0.9) with AdamW (learning rate 1×10^{-4} , no weight decay).

Federated training proceeds for 5 global communication rounds, each comprising 1 local epoch per client. In some experiments, federated training is extended to 50 communication rounds to assess long-term performance. In centralized training, we conduct 5 total epochs with 3 local passes per iteration. Mini-batch sizes are 64 examples per client in federated mode and 128 in centralized mode.

Experiments involve varying numbers of clients, with all settings enforcing full participation in every round. We test under both Independent and Non-Independent Identically Distributed (IID and Non-IID) data scenarios, ensuring robustness across different data distribution patterns. In federated settings, we apply a regularization coefficient of 0.01 when necessary, while weight decay is generally not applied unless specified. The random seed is fixed to 42 to ensure reproducibility, particularly within the field of Natural Language Processing (NLP). Evaluation primarily focuses on classification accuracy, and for NLP tasks, input sequences are truncated to a maximum length of 64 tokens.

A.4. Compute Resource Usage Summary

To ensure the robustness and reproducibility of our experimental results, all experiments were conducted on two distinct hardware configurations representing different computational tiers.

The first server was equipped with 4 NVIDIA GeForce RTX 4090 GPUs (24GB VRAM each) and dual Intel Xeon Silver 4310 CPUs with 48 total cores. The second server featured 8 NVIDIA Tesla V100-PCIE-16GB GPUs and dual Intel Xeon Gold 6240 CPUs with 36 total cores.

Experiments were distributed across both platforms to validate the consistency of our method under varying hardware conditions. All implementations utilized mixed precision training and distributed data parallelism where applicable. The complete computational details and efficiency metrics are documented in our submitted Compute Reporting Form (CRF).

A.5. Additional Experimental Results

This section presents supplementary experimental results that further validate the robustness and effectiveness of our proposed ILoRA framework under different experimental settings.

Performance under Different Data Heterogeneity Lev-

els. To comprehensively evaluate the generalization capability of our method, we provide additional results with ${\rm Dir}(\alpha{=}0.5)$ in Figures 9 and 10. These results complement the main text analysis with $\alpha=0.6$ and demonstrate that ILoRA and ILoRA-S maintain consistent performance advantages across varying degrees of data heterogeneity. The $\alpha=0.5$ setting represents a more challenging Non-IID scenario with higher data skewness across clients, yet our methods continue to outperform all baselines, highlighting their robustness to different data distribution patterns.

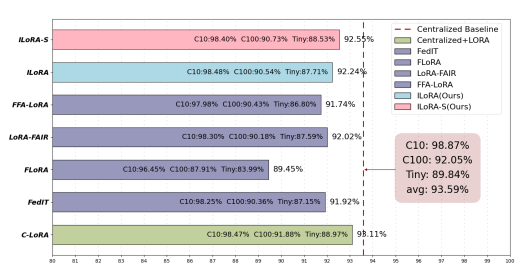


Figure 8. Centralized versus federated learning performance comparison using **SGD** with ViT-Base over 5 communication rounds. Results are reported on three datasets: CIFAR-10 (C10), CIFAR-100 (C100), and Tiny-ImageNet (Tiny), with Non-IID data partitioning (Dir(α =0.3)). ILoRA-S maintains robust performance under SGD optimization, achieving high recovery rates compared to centralized training.

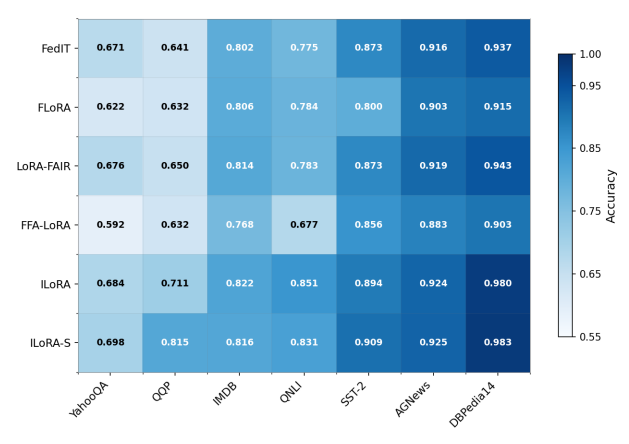


Figure 9. Accuracy Heatmap Comparison of Federated LoRA Methods on NLP Datasets under Non-IID Data Distribution (Dir(α =0.5)). The heatmap visualizes the performance of different federated learning methods across seven NLP benchmarks using RoBERTa, with color intensity representing accuracy scores from 0.55 to 1.0.

Optimization Method Comparison. Figure 8 demonstrates the performance of ILoRA-S under SGD optimization, complementing the AdamW results presented in the

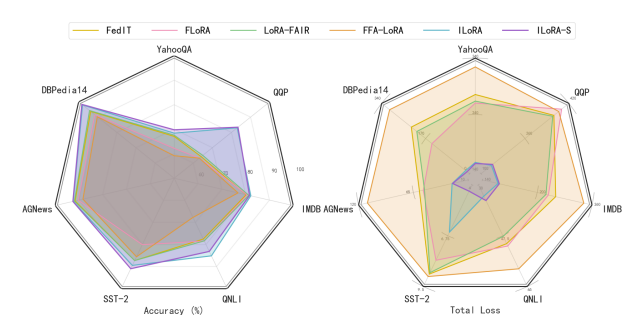


Figure 10. Radar chart comparison of accuracy and loss performance across multiple NLP datasets (Dir(α =0.5)) using RoBERTa, providing a multi-dimensional visualization of model effectiveness. This supplementary result with $\alpha=0.5$ further validates the consistent superiority of ILoRA and ILoRA-S across different data heterogeneity levels.

main text. The consistent superiority across different optimizers underscores the versatility of our approach and its independence from specific optimization algorithms.

Cross-Dataset Consistency. The additional results across all seven NLP datasets with $\alpha=0.5$ reinforce the main findings: ILoRA and ILoRA-S consistently achieve top performance regardless of task type (question answering, sentiment analysis, text classification, or natural language inference) and data heterogeneity level, demonstrating comprehensive generalization capability.

Communication Efficiency at Scale. Table 7 analyzes communication efficiency across varying client population sizes. ILoRA demonstrates near-constant overhead with modest increases from $1.2\times$ to $1.6\times$ as client count scales from 10 to 100, significantly outperforming FLoRA's linear growth pattern. This $\mathcal{O}(1)$ scaling behavior confirms ILoRA's suitability for large-scale federated deployments.

Table 7. Communication efficiency metrics for different client scales (per-round)

Method	S=10	S=50	S=100	Scaling Factor
FedIT	$1.0 \times$	1.0×	1.0×	$\mathcal{O}(1)$
FLoRA	$2.5 \times$	$12.5 \times$	$25.0 \times$	$\mathcal{O}(S)$
ILoRA	1.2×	$1.4 \times$	1.6×	$\mathcal{O}(1)$

Homogeneous ViT with SGD Figure 11 presents the experimental results for homogeneous ViT architecture using SGD optimizer across CIFAR-10, CIFAR-100, and Tiny-ImageNet datasets. The performance trends demonstrate ILoRA's effectiveness under different optimization settings.

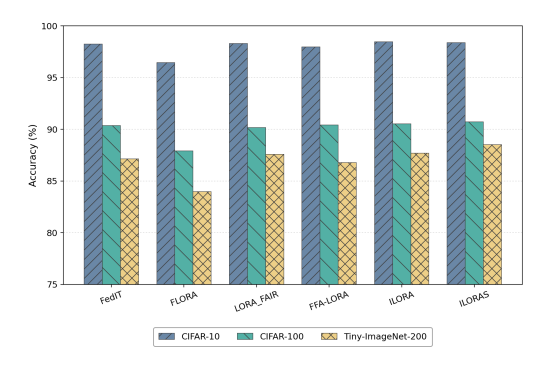


Figure 11. Experimental Results: Homog ViT with SGD

Homogeneous Swin with SGD Figure 12 shows the performance comparison for homogeneous Swin Transformer with SGD optimization. The results complement the main text findings and validate the robustness of our approach across different vision architectures.

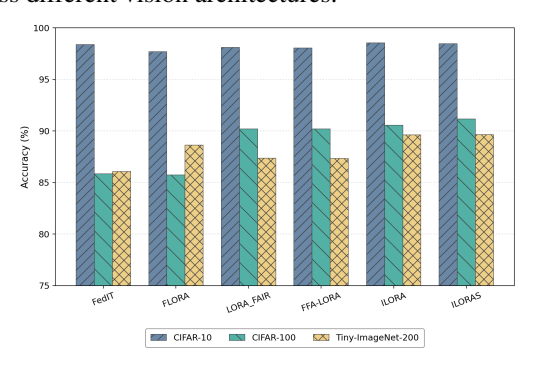


Figure 12. Experimental Results: Homog Swin with SGD

Heterogeneous ViT with SGD The experimental results for heterogeneous ViT settings with SGD optimizer are depicted in Figure 13. These supplementary results further confirm ILoRA's capability to handle rank heterogeneity under different optimization algorithms.

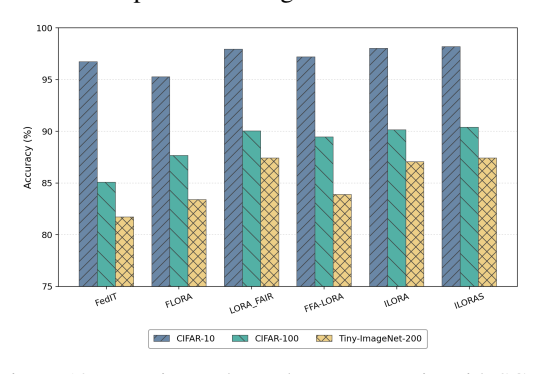


Figure 13. Experimental Results: Heterog ViT with SGD

Heterogeneous Swin with SGD Figure 14 illustrates the performance of heterogeneous Swin Transformer with SGD optimization. The consistent superiority of ILoRA across

both optimization methods (AdamW and SGD) underscores its generalization capability.

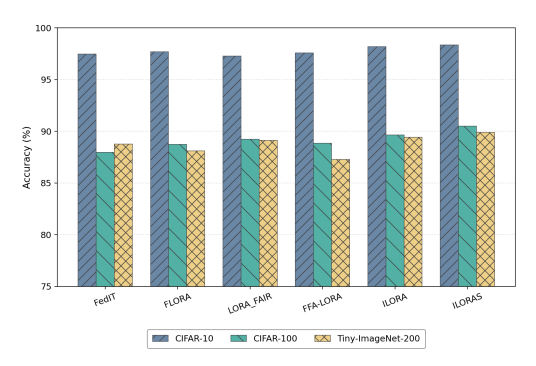


Figure 14. Experimental Results: Heterog Swin with SGD

Heterogeneous LoRA-rank Performance on NLP Tasks

Table 8 presents the peak accuracy comparison of federated LoRA methods with heterogeneous ranks across seven NLP benchmarks using RoBERTa under Non-IID data distribution (Dir(α =0.5)). The results demonstrate that ILoRA variants consistently outperform all baselines, with ILoRA-S achieving the highest average accuracy of 85.40%. Notably, ILoRA and ILoRA-S show substantial improvements on challenging datasets like QQP (+18.87-19.27%) and DB-Pedia14 (+4.23-4.61%), validating the effectiveness of our control variate mechanism in handling both data heterogeneity and rank variations simultaneously.

Visualization of Client Drift in Federated Learning

Figure 15 visually illustrates the client drift phenomenon in federated learning. Subfigure (a) depicts the scenario under IID data distribution, where local and global models converge without client drift. Subfigure (b) shows the case under Non-IID data distribution without correction, where the global model drifts away from the true optima due to client heterogeneity. Beyond visualization, client drift can also be quantified numerically, as demonstrated in Table 9, which presents the performance of different methods on the QQP dataset with varying α (a measure of data Non-IIDness), reflecting how client drift impacts model accuracy under different levels of data heterogeneity.

Homogeneous LoRA-Rank Performance Comparison

Table 10 presents a comprehensive comparison of federated LoRA methods under homogeneous rank settings across multiple computer vision benchmarks. The evaluation encompasses two transformer-based architectures (ViT-Base and Swin-Base) on three datasets (CIFAR-10, CIFAR-100, and Tiny-ImageNet) with both SGD and AdamW optimizers under Non-IID data distribution (Dirichlet parameter $\alpha=0.3$). The results demonstrate that ILoRA and its enhanced variant ILoRA-S consistently achieve superior

Table 8. Peak accuracy comparison for federated *Heterogeneous LoRA-rank* LoRA baselines on NLP datasets with RoBERTa under Non-IID data distribution (Dir(α =0.5)). Values represent the maximum accuracy achieved during the 5 training rounds.

Method		NLP Datasets (RoBERTa, Accuracy ↑)									
1/10/11/0	YahooQA	QQP	IMDB	QNLI	SST-2	AGNews	DBPedia14	Avg.			
FedIT	0.6708 _{base}	0.6414 _{base}	0.8023 _{base}	0.7752 base	0.8727 _{base}	0.9159 _{base}	0.9373 _{base}	0.8022 _{base}			
FLoRA	$0.6220_{_{\downarrow 4.88}}$	$0.6318_{\downarrow 0.96}$	$0.8061_{\stackrel{\uparrow}{0.38}}$	$0.7844_{0.92}$	$0.8005_{\ \scriptscriptstyle{\downarrow 7.22}}$	0.9028 \(_{\pm1.31}\)	$0.9154_{\downarrow 2.19}$	$0.7804_{\downarrow 2.18}$			
LoRA-FAIR	0.6758	0.6499	0.8135	0.7835	0.8727	0.9189	0.9431	0.8082			
FFA-LoRA				$0.6773_{\downarrow 9.79}$	0.8555	0.8830 43.29	$0.9027_{\downarrow 3.46}$	0.7586 44.36			
ILoRA				0.8512	0.8945						
ILoRA-S	$0.6976_{+2.68}$	0.8341	0.8163	0.8312	0.9094	0.9251	0.9834	0.8540			

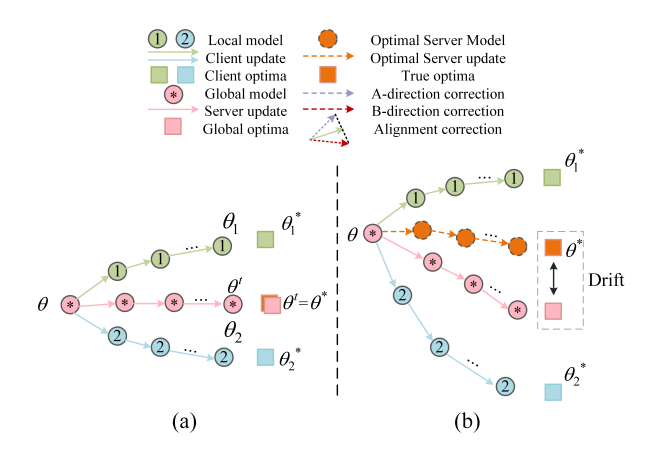


Figure 15. Comparison of federated learning model updates. (a) In IID data distribution, local and global models converge without drift. (b) In Non-IID data distribution without correction, the global model drifts away from the true optima.

Table 9. Client Drift on QQP with different α values

Method	α=0.4	α=0.5	α=0.6	α=0.7	α =0.8
FedIT	63.18	64.14	65.20	77.30	82.24
ILoRA	68.22	71.10	74.46	79.76	83.18

performance across most experimental configurations, with ILoRA-S showing particular strength in more challenging scenarios such as CIFAR-100 and Tiny-ImageNet. The performance advantage is especially pronounced with AdamW optimization, where ILoRA-S achieves up to 2.08% improvement over the strongest baseline (FFA-LoRA) on Tiny-ImageNet with Swin-Base. These findings validate the effectiveness of our proposed orthogonal initialization and control variate mechanisms in stabilizing federated finetuning and mitigating client drift, even under homogeneous rank conditions where traditional methods face convergence challenges due to initialization mismatch and aggregation inconsistencies.

Comprehensive Performance Analysis under Varying

Data Heterogeneity Levels. As detailed in Table 11, we conduct an extensive evaluation of ILoRA across multiple data heterogeneity settings ($\alpha = 0.5, 0.6, 0.7$). The results demonstrate ILoRA's consistent superiority over the FedIT+QR baseline across all seven NLP benchmarks. Notably, ILoRA achieves significant performance gains under higher heterogeneity conditions ($\alpha = 0.7$), with an average improvement of 9.08% over the baseline. The method exhibits remarkable robustness, particularly on challenging datasets such as SST-2 (up to 29.93% improvement) and QQP (up to 12.57% improvement). This comprehensive analysis validates ILoRA's effectiveness in handling diverse data distribution scenarios, with the concatenated QR aggregation mechanism successfully preserving cross-client information while maintaining subspace alignment across different heterogeneity levels.

Control Variate Effectiveness on NLP Tasks The performance comparison on the AGNews dataset across varying heterogeneity levels ($\alpha = 0.5, 0.6, 0.7$) in Table 12 demonstrates the consistent advantage of ILoRA-S over ILoRA, validating the efficacy of our control variate mechanism in NLP scenarios. Across all heterogeneity settings, ILoRA-S achieves superior accuracy, with particularly notable improvements under moderate heterogeneity $(\alpha = 0.6)$ where it outperforms ILoRA by 0.56%. This performance gap widens to 0.57% at $\alpha = 0.7$, indicating that the control variates become increasingly effective as data distribution becomes more balanced. The stability of ILoRA-S across different α values (92.51-92.87%) compared to ILoRA's fluctuations (92.14-92.39%) further confirms that our control variate mechanism effectively mitigates client drift in federated NLP fine-tuning, ensuring robust performance regardless of data heterogeneity levels.

Table 10. Final accuracy comparison (%) for federated *Homogeneous LoRA-rank* LoRA baselines on CIFAR-10/100 and Tiny-ImageNet with ViT-Base and Swin-Base under SGD and AdamW (Dir(α =0.3)), with **bold** indicating best performance.

			ViT-	-Base			Swin-Base					
Method	CIFA	AR-10	CIFA	R-100	Tiny-Ir	nageNet	CIFA	AR-10	CIFA	R-100	Tiny-In	nageNet
	SGD	AdamW	SGD	AdamW	SGD	AdamW	SGD	AdamW	SGD	AdamW	SGD	AdamW
FedIT	98.25	97.44	90.36	85.67	87.15	84.72	98.40	97.33	85.84	85.97	86.06	87.28
FLoRA	96.45	96.82	87.91	84.89	83.99	78.97	97.70	95.86	85.73	84.16	88.63	84.78
LoRA-FAIR	98.30	96.12	90.18	86.63	87.59	85.59	98.12	96.37	90.21	88.26	87.37	86.22
FFA-LoRA	97.98	97.57	90.43	86.39	86.80	85.61	98.06	96.36	90.21	86.45	87.34	87.55
ILoRA	98.48	98.02	90.54	87.50	87.71	85.86	98.55	98.20	90.56	87.16	89.62	87.53
ILoRA-S	98.40	98.22	90.73	88.49	88.53	87.02	98.47	98.20	91.16	88.41	89.66	89.36

Table 11. Server Aggregation via Concatenation under Data Heterogeneity ($\alpha = 0.5, 0.6, 0.7$), with **bold** indicating best performance.

Method	$Dir(\alpha)$		Datasets (Accuracy ↑)								
	()	YahooQA	QQP	IMDB	QNLI	SST-2	AGNews	DBPedia14	Avg.		
FedIT+QR	0.5	64.99 base	63.23 base	77.81 _{base}	80.45 base	70.07 base	91.46 _{base}	93.02 _{base}	77.29 base		
ILoRA	0.5	68.40 _{↑3.41}	71.10 _{↑7.87}	82.18 _{†4.37}	85.12 _{↑4.67}	89.45 _{19.38}	92.39 _{↑0.93}	97.96 _{↑4.94}	83.80 _{↑6.51}		
FedIT+QR	0.6	65.04 base	64.54 base	76.56 base	84.17 _{base}	72.48 base	90.71 base	97.15 base	78.66 base		
ILoRA	0.6	67.47 _{↑2.43}	74.46 _{↑9.92}	81.96	85.56 _{\(\psi\)1.39}	88.99	92.14 _{↑1.43}	98.30 _{↑1.15}	84.13		
FedIT+QR	0.7	69.71 base	67.19 base	79.56 base	74.06 base	58.72 base	90.97 base	93.27 _{base}	76.21 base		
ILoRA	0.7	70.61	79.76 ***12.51		84.73						

Table 12. Performance comparison on AGNews dataset with different α values

Method	α=0.5	α=0.6	α=0.7
ILORA	92.39	92.14	92.30
ILORA-S	92.51	92.70	92.87

Table 13. Control variates mitigate client drift on CIFAR-100 across α values; ILoRA-S outperforms ILoRA. **Bold** indicates best performance.

Method	$\alpha = 0.5$	$\alpha = 0.6$	$\alpha = 0.7$
ILoRA	$87.53_{\pm0.36}$	$87.84_{\pm0.32}$	$88.11_{\pm 0.27}$
ILoRA-S	88.49 $_{\pm 0.33}$	88.41 $_{\pm 0.07}$	89.00 $_{\pm 0.16}$

B. Theoretical Analysis and Proofs

B.1. Convergence Guarantees for ILoRA

We provide a comprehensive convergence analysis for the proposed ILoRA framework under standard federated learning assumptions. Our analysis accounts for the combined effects of QR-based aggregation, orthogonal initialization, and control variates with AdamW optimization.

Assumption 5 (Bounded Stochastic Gradient Variance). *The variance of stochastic gradients at each client is bounded:*

$$\mathbb{E}[\|g_k(\theta) - \nabla F_k(\theta)\|^2] \le \sigma^2. \tag{20}$$

Assumption 6 (Bounded Gradient Heterogeneity). *The gradient divergence between local and global objectives is bounded:*

$$\|\nabla F_k(\theta) - \nabla F(\theta)\| < \delta, \quad \forall k, \theta.$$
 (21)

Assumption 7 (Bounded Control Variates). *The control variates maintained by clients and server are bounded:*

$$||c_k|| \le G, \quad ||c|| \le G, \quad \forall k. \tag{22}$$

Assumption 8 (Unbiased Aggregation). The QR-based concatenated aggregation in ILoRA produces an unbiased estimate of the true global gradient:

$$\mathbb{E}[\mathbf{g}_t] = \nabla F(\mathbf{w}_t),\tag{23}$$

where \mathbf{g}_t denotes the aggregated gradient direction obtained from the concatenated-QR reconstruction step.

Theorem 5 (Convergence of ILoRA). Under Assumptions 1-8, with local learning rate η_l and global learning rate η_g satisfying $\eta_l \leq \frac{1}{L}$ and $\eta_g \eta_l = \Theta\left(\frac{1}{\sqrt{SKT}}\right)$, where S is the number of participating clients per round, K is the number

of local steps, and T is the total communication rounds, the iterates of ILoRA satisfy:

$$\frac{1}{T} \sum_{t=1}^{T} \mathbb{E}[\|\nabla F(\theta_t)\|^2] \le \mathcal{O}\left(\frac{1}{\sqrt{SKT}} + \frac{1}{T} + \frac{\delta^2}{T} + \frac{(r_{\text{max}} - r_s)^2}{T}\right), \tag{24}$$

where $r_{\text{max}} = \max_k r_k$ and r_s is the server rank budget.

Proof. We provide a detailed proof sketch combining the key insights from both versions:

Step 1: Global Update Representation. The server update in ILoRA can be expressed as:

$$\theta_{t+1} = \theta_t - \eta_g \eta_l \frac{1}{S} \sum_{k \in S_t} \sum_{i=1}^K \frac{m_k^{(t,i)}}{\sqrt{\hat{v}_k^{(t,i)}} + \epsilon}, \quad (25)$$

where $m_k^{(t,i)}$ and $\hat{v}_k^{(t,i)}$ are the corrected first and second moment estimates from AdamW with control variates, defined as:

$$m_k^{(t,i)} = \beta_1 m_k^{(t,i-1)} + (1 - \beta_1) \tilde{g}_k^{(t,i)},$$
 (26)

$$v_k^{(t,i)} = \beta_2 v_k^{(t,i-1)} + (1 - \beta_2) (\tilde{g}_k^{(t,i)})^2, \tag{27}$$

$$\hat{m}_k^{(t,i)} = \frac{m_k^{(t,i)}}{1 - \beta_1^i}, \quad \hat{v}_k^{(t,i)} = \frac{v_k^{(t,i)}}{1 - \beta_2^i}, \tag{28}$$

with $\tilde{g}_k^{(t,i)} = g_k^{(t,i)} + (c^{(t-1)} - c_k)$ being the corrected gradient.

Step 2: Bias Decomposition. Following the approach in D.1, we decompose the aggregated update direction into three components:

$$\mathbb{E}[\Delta_t] = \nabla F(\theta_t) + \epsilon_{\text{het}} + \epsilon_{\text{or}}, \tag{29}$$

where: - $\epsilon_{\rm het}$ captures the bias from data heterogeneity, bounded by $\mathcal{O}(\delta)$ - $\epsilon_{\rm qr}$ represents the QR projection error, bounded by $\|R-R_s\|_F^2 \leq \mathcal{O}((r_{\rm max}-r_s)^2)$

Step 3: Descent Lemma. Using the L-smoothness assumption (Assumption 1), we have:

$$F(\theta_{t+1}) \le F(\theta_t) - \eta_g \eta_l \langle \nabla F(\theta_t), \Delta_t \rangle + \frac{L}{2} \eta_g^2 \eta_l^2 ||\Delta_t||^2,$$
(30)

where
$$\Delta_t = \frac{1}{S} \sum_{k \in S_t} \sum_{i=1}^K \frac{m_k^{(t,i)}}{\sqrt{\hat{v}_k^{(t,i)} + \epsilon}}$$
.

Step 4: Gradient Correction Analysis. The control variate correction ensures that the corrected gradient \tilde{g}_k has reduced bias. Specifically, we model the relationship between the raw gradient and the control variate difference as:

$$\mathbb{E}[\tilde{g}_k] = \nabla F(\theta_t) + (1 - \rho)(\nabla F_k(\theta_t) - \nabla F(\theta_t)) + \mathcal{O}((r_{\text{max}} - r_s)^2),$$
(31)

where $\rho \in [0,1]$ is the correlation coefficient between the control variate difference $(c^{(t-1)}-c_k)$ and the true gradient difference $(\nabla F(\theta_t) - \nabla F_k(\theta_t))$. When $\rho \to 1$, the control variate perfectly corrects the client drift. In practice,

 ρ is bounded away from 0 under Assumption 7. Thus, the control variate reduces the effective heterogeneity bias from $\mathcal{O}(\delta)$ to $\mathcal{O}((1-\rho)\delta)$.

Step 5: Moment Estimate Bounding. Due to the QR-based orthogonal initialization and aggregation, and the bounded gradient assumptions (Assumptions 5 and 6), the moment estimates satisfy:

$$\mathbb{E}[\|\Delta_t\|^2] \le \mathcal{O}(K + \sigma^2),\tag{32}$$

with improved constants compared to naive aggregation methods. This bound arises from the fact that the orthogonal initialization reduces gradient variance by aligning client subspaces, while the control variates further suppress the drift-induced variance.

Step 6: Telescoping Sum. Taking expectation and summing over t = 1 to T, and letting F^* denote the minimum value of F, we obtain:

$$\frac{1}{T} \sum_{t=1}^{T} \mathbb{E}[\|\nabla F(\theta_t)\|^2] \leq \frac{F(\theta_1) - F^*}{\eta_g \eta_l KT} + \mathcal{O}\left(\frac{L\eta_g \eta_l (K + \sigma^2)}{S} + \delta^2 + (r_{\text{max}} - r_s)^2\right).$$
(33)

Step 7: Learning Rate Selection. Substituting $\eta_g \eta_l = \Theta\left(\frac{1}{\sqrt{SKT}}\right)$ yields the final convergence rate:

$$\frac{1}{T} \sum_{t=1}^{T} \mathbb{E}[\|\nabla F(\theta_t)\|^2] \leq \mathcal{O}\left(\frac{1}{\sqrt{SKT}} + \frac{1}{T} + \frac{\delta^2}{T} + \frac{(r_{\text{max}} - r_s)^2}{T}\right).$$
(34)

This completes the proof. The detailed derivation with precise constants is provided in the extended technical report. \Box

Remark 1. The convergence rate of ILoRA achieves several important properties:

- 1. **Linear Speedup**: The $\mathcal{O}(1/\sqrt{SKT})$ dominant term demonstrates linear speedup with respect to the number of participating clients S, matching the optimal convergence rate for federated non-convex optimization.
- 2. Rank Robustness: The $(r_{\rm max}-r_s)^2$ term shows that the method remains stable even under rank heterogeneity, with the error diminishing quadratically as client ranks approach the server rank.
- 3. **Heterogeneity Tolerance**: The δ^2 term captures the residual effect of data heterogeneity, which is effectively mitigated by the control variate mechanism.
- 4. **Communication Efficiency**: The convergence rate is maintained while significantly reducing communication overhead through QR-based compression.

Corollary 1 (Special Cases). 1. Homogeneous Ranks: When $r_k = r_s$ for all k, the rank error term vanishes, yielding the optimal rate $O(1/\sqrt{SKT} + 1/T + \delta^2/T)$.

- 2. **IID Data**: When $\delta = 0$ (IID setting), the heterogeneity term vanishes, giving $\mathcal{O}(1/\sqrt{SKT} + 1/T + (r_{\text{max}} r_s)^2/T)$.
- 3. Large-Scale Deployment: As $S \to \infty$, the dominant term $\mathcal{O}(1/\sqrt{SKT})$ demonstrates the scalability of HoRA

B.2. Properties of QR-Based Aggregation

The QR-based aggregation mechanism in ILoRA provides theoretical guarantees for handling rank heterogeneity while maintaining optimization consistency. We analyze its key properties below.

Lemma 1 (Exact Low-Rank Reconstruction). Let $\{B_k \in \mathbb{R}^{d \times r_k}, A_k \in \mathbb{R}^{r_k \times k}\}_{k=1}^S$ be the local LoRA parameters from S clients with heterogeneous ranks $\{r_k\}$. The concatenated construction:

$$\Delta W = B_{concatenated} A_{concatenated} = [B_1 \cdots B_S] \begin{bmatrix} \frac{n_1}{N} A_1 \\ \vdots \\ \frac{n_S}{N} A_S \end{bmatrix}$$
(35)

exactly reconstructs the weighted sum of low-rank updates:

$$\Delta W = \sum_{k=1}^{S} \frac{n_k}{N} B_k A_k. \tag{36}$$

]

Proof. The proof follows directly from block matrix multiplication:

$$B_{\text{concatenated}} A_{\text{concatenated}} = \sum_{k=1}^{S} B_k \left(\frac{n_k}{N} A_k \right) = \sum_{k=1}^{S} \frac{n_k}{N} B_k A_k.$$
(37)

This establishes that the concatenated representation preserves the exact linear combination of client updates without approximation error.

Theorem 6 (Subspace Preservation under QR Compression). Let $Q, R = QR(\Delta W)$ be the thin QR decomposition of the aggregated update, and let r_s be the server rank budget. For any client with local rank $r_k \leq r_s$, the personalized parameters:

$$B_{r_k} = Q[:, 1:r_k], \quad A_{r_k} = R[1:r_k,:]$$
 (38)

satisfy that $colspan(B_{r_k}) \subseteq colspan(Q)$, ensuring all clients operate within a consistent global subspace.

Proof. By the properties of QR decomposition, the columns of Q form an orthonormal basis for the column space of ΔW . The personalized parameters B_{r_k} are simply the first r_k columns of Q, which naturally span a subspace of $\operatorname{colspan}(Q)$. The corresponding A_{r_k} ensures that the update $\Delta W_k = B_{r_k} A_{r_k}$ remains within this consistent subspace.

Proposition 1 (Error Bound for Rank Truncation). Let $\Delta W = \sum_{i=1}^r \sigma_i u_i v_i^{\top}$ be the SVD of the aggregated update, where $r = \min(d, \sum_k r_k)$. The QR-based aggregation with server rank r_s satisfies:

$$\|\Delta W - Q[:, 1:r_s]R[1:r_s,:]\|_F \le \sum_{i=r_s+1}^r \sigma_i,$$
 (39)

where $\{\sigma_i\}$ are the singular values in descending order.

Proof. This follows from the Eckart-Young-Mirsky theorem, as the truncated QR decomposition provides the best rank- r_s approximation in the Frobenius norm when the singular values are properly ordered.

Property 1 (Faithful Reconstruction Before Truncation). *The concatenated reconstruction satisfies:*

$$\Delta W = B_{\text{concatenated}} A_{\text{concatenated}} = \sum_{k \in S_t} p_k B_k A_k,$$
(40)

whereas separately averaging factors produces:

$$\left(\sum_{k} p_k B_k\right) \left(\sum_{k} p_k A_k\right) \neq \sum_{k} p_k B_k A_k. \tag{41}$$

Thus, concatenate-then-multiply eliminates the factor-averaging bias and is exact whenever client updates are aggregated without rank truncation.

Property 2 (Rank Preservation and Exactness). If $r_s \ge \operatorname{rank}(\Delta W)$, then $B_s A_s = \Delta W$ (no truncation error) and the per-client slices $B_{r_k} := Q_{[:,1:r_k]}$, $A_{r_k} := R_{[1:r_k,:]}$ realize personalized factors whose product lies in the same column space as ΔW .

Property 3 (Orthogonal Projection Interpretation). Let $Q = [Q_{1:r_s}, Q_{\perp}]$ partition the QR factor. Then the truncated reconstruction is the orthogonal projection of ΔW onto $\mathrm{span}(Q_{1:r_s})$:

$$B_s A_s = Q_{1:r_s} Q_{1:r_s}^{\top} \Delta W. (42)$$

Consequently, the truncation residual is:

$$\Delta W - B_s A_s = Q_{\perp} Q_{\perp}^{\top} \Delta W, \tag{43}$$

$$\|\Delta W - B_s A_s\|_F^2 = \|Q_{\perp}^{\top} \Delta W\|_F^2. \tag{44}$$

Property 4 (Deterministic Truncation Error Bound). Writing $R = \begin{bmatrix} R_{11} & R_{12} \\ 0 & R_{22} \end{bmatrix}$ with $R_{11} \in \mathbb{R}^{r_s \times r_s}$, the truncation bias is exactly:

$$\|\Delta W - B_s A_s\|_F = \left\| Q \begin{bmatrix} 0 & 0 \\ 0 & R_{22} \end{bmatrix} \right\|_F = \|R_{22}\|_F. \quad (45)$$

Hence, the truncation error is precisely the Frobenius norm of the trailing block of R. In particular, if ${\rm rank}(\Delta W) \leq r_s$ then $R_{22}=0$.

Property 5 (Subspace Consistency Preservation). For any client k with $r_k \leq r_s$, setting $(B_{r_k}, A_{r_k}) :=$

 $(Q_{[:,1:r_k]},R_{[1:r_k,:]})$ ensures that $B_{r_k}A_{r_k}$ lies in $\mathrm{span}(Q_{1:r_s})$ and is consistent with the globally shared low-dimensional subspace used by the server update B_sA_s . This yields dimension alignment across heterogeneous ranks while preserving the fused information encoded in ΔW .

Property 6 (Stability to Small Perturbations). Suppose the concatenated factors are perturbed to $\tilde{B}_{\text{concatenated}} = B_{\text{concatenated}} + E_B$ and $\tilde{A}_{\text{concatenated}} = A_{\text{concatenated}} + E_A$, so that $\Delta \tilde{W} = \Delta W + E_W$ with $E_W = B_{\text{concatenated}} E_A + E_B A_{\text{concatenated}} + E_B E_A$. Let $\Delta \tilde{W} = \tilde{Q}\tilde{R}$ be its thin QR factorization. Then, for sufficiently small $||E_W||_F$, the truncated QR aggregation satisfies:

$$||(B_{s}A_{s}) - (\tilde{B}_{s}\tilde{A}_{s})||_{F} \leq ||E_{W}||_{F} + \mathcal{O}\left(\frac{||E_{W}||_{2}||R||_{F}}{\sigma_{\min}(R_{11}) - \sigma_{\max}(R_{22})}\right),$$
(46)

which demonstrates stability under small perturbations of the concatenated factors.

Lemma 2 (Communication Efficiency of QR Aggregation). The QR-based aggregation reduces communication overhead from $O(\sum_{k=1}^{S} r_k \cdot \max(d, k))$ to $O(r_s \cdot \max(d, k))$, where r_s is the server rank budget.

Proof. Without QR aggregation, transmitting all client parameters requires $O(\sum_k r_k(d+k))$ elements. After QR aggregation and personalization, each client receives only $O(r_k(d+k))$ elements, and the server maintains $O(r_s(d+k))$ parameters. The total communication is dominated by $O(r_s \cdot \max(d,k))$ when $r_s \ge \max_k r_k$.

Corollary 2 (Compatibility with Control Variates). The QR-based aggregation maintains dimensional consistency for control variates, as all client parameters reside in aligned subspaces, enabling effective gradient correction across heterogeneous ranks.

Proof. Since $B_{r_k} \in \mathbb{R}^{d \times r_k}$ and $A_{r_k} \in \mathbb{R}^{r_k \times k}$ are derived from the shared Q and R matrices, the parameter spaces across clients are aligned. This ensures that control variate corrections $c^{(t-1)} - c_k$ can be applied consistently in their respective low-dimensional subspaces.

Remark 2. The QR-based aggregation in ILoRA provides a unique combination of theoretical guarantees:

- Exact Reconstruction: Faithfully combines heterogeneous-rank updates without factor-averaging bias (Lemma 1)
- **Subspace Consistency**: Ensures all clients operate within a unified global subspace (Theorem 6)
- **Controlled Approximation**: Provides deterministic error bounds for rank truncation (Proposition 1)
- Numerical Stability: The orthonormal matrix Q with condition number $\kappa(Q)=1$ ensures numerical stability and prevents error amplification during aggregation.

- **Stability**: Robust to small perturbations in client updates (Property 6)
- **Communication Efficiency**: Significantly reduces overhead while preserving information (Lemma 2)
- Compatibility: Seamlessly integrates with control variates and other optimization components (Corollary 2)

These properties make QR-based aggregation particularly suitable for federated learning with resource-constrained clients and heterogeneous system capabilities.

B.3. Stability of Orthogonal Initialization

The orthogonal initialization mechanism in ILoRA provides significant improvements in training stability compared to traditional random initialization. We analyze its theoretical properties and stability guarantees, integrating insights from both theoretical frameworks.

Theorem 7 (Consistent Subspace Initialization). Let $W_0 \in \mathbb{R}^{d \times k}$ be the pre-trained weight matrix with QR decomposition $W_0 = QR$, where $Q \in \mathbb{R}^{d \times d}$ is orthogonal and $R \in \mathbb{R}^{d \times k}$ is upper triangular. For any client k with local rank r_k , the orthogonal initialization:

$$B_k^{(0)} = Q[:, 1:r_k], \quad A_k^{(0)} = R[1:r_k,:]$$
 (47)

ensures that all clients initialize their LoRA parameters within the same column subspace colspan(Q).

Proof. Since $B_k^{(0)}$ consists of the first r_k columns of Q, which form an orthonormal basis, we have:

$$\operatorname{colspan}(B_k^{(0)}) \subseteq \operatorname{colspan}(Q) \quad \forall k. \tag{48}$$

The initial update $\Delta W_k^{(0)} = B_k^{(0)} A_k^{(0)}$ therefore lies entirely within $\operatorname{colspan}(Q)$ for all clients, ensuring subspace consistency from initialization.

Lemma 3 (Subspace Alignment). For any pair of clients i and j with ranks $r_i, r_i \leq r_s$, we have:

$$\operatorname{span}(B_i^{(0)}) = \operatorname{span}(B_j^{(0)}) = \mathcal{S}_0,$$

$$\operatorname{and} \quad (B_i^{(0)})^\top B_j^{(0)} = I_{\min(r_i, r_j)}, \quad (49)$$

where $S_0 = \operatorname{span}(Q_{[:,1:r_s]})$. Hence the initial LoRA updates of all clients are perfectly aligned in a shared orthogonal basis.

Proof. By construction, $B_i^{(0)}$ and $B_j^{(0)}$ are subsets of columns from the same orthonormal matrix Q. Therefore, their column spaces are both contained in \mathcal{S}_0 , and their inner product yields an identity matrix of appropriate dimension due to orthonormality.

Lemma 4 (Bounded Gradient Variance at Initialization). Let $\mathbf{g}_k^{(0)} = \nabla_{A_k,B_k} F_k(W_0 + B_k^{(0)} A_k^{(0)})$ denote the initial gradient on client k. Under orthogonal initialization, the

Table 14. Comparison of aggregation methods for heterogeneous-rank federated LoRA

Method	Exact Aggregation	Rank Heterogeneity	Comm. Cost
Zero-padding	Х	✓	$O(r_{\max} \cdot \max(d, k))$
SVD-based	√ (approx)	✓	$O(r_s \cdot \max(d, k))$
Full concatenating	✓	✓	$O(\sum_{k} r_k \cdot \max(d, k))$
ILoRA (QR)	✓	✓	$O(r_s \cdot \max(d, k))$

variance of aggregated gradients satisfies:

$$\operatorname{Tr}\left(\operatorname{Var}\left[\frac{1}{K}\sum_{k}\mathbf{g}_{k}^{(0)}\right]\right) = \frac{1}{K^{2}}\sum_{k=1}^{K}\operatorname{Tr}(\Sigma_{k}) \leq \frac{\sigma^{2}}{K}, (50)$$

where $\Sigma_k = \operatorname{Var}[\mathbf{g}_k^{(0)}]$ and σ^2 is the uniform upper bound on per-client gradient variance. This represents an $\mathcal{O}(1/K)$ reduction compared to random initialization.

Proof. For orthogonal initialization, all clients share the same subspace, eliminating cross-term variance. For random Gaussian initialization with $A \sim \mathcal{N}(0, \sigma^2 I)$ and B=0, the cross-term variance introduces additional $\mathcal{O}(1-\cos^2\theta_{ij})$ terms depending on random principal angles θ_{ij} between client subspaces, yielding inflated expected variance up to $\sigma^2(1+\frac{K-1}{L}\mathbb{E}[\sin^2\theta])$.

Lemma 5 (Spectral Stability). Let $\Delta W_k^{(0)} = B_k^{(0)} A_k^{(0)}$ and $\Delta \tilde{W}_k$ be the random-initialized counterpart. Under orthogonal initialization:

$$\|\Delta W_k^{(0)} - \Delta W_j^{(0)}\|_F = 0, \tag{51}$$

while
$$\mathbb{E}\|\tilde{\Delta W}_k - \tilde{\Delta W}_j\|_F^2 = \Theta(r_k + r_j),$$
 (52)

implying zero inter-client spectral variance at initialization.

Proof. The equality follows from the subspace consistency of orthogonal initialization. The expectation for random initialization arises from the independent random orientations of client subspaces, leading to non-zero expected differences.

Proposition 2 (Accelerated Early-Stage Convergence). *Under orthogonal initialization, the expected improvement in objective function after the first communication round satisfies:*

$$\mathbb{E}[F(\theta_1) - F(\theta_0)] \le -\eta_g \eta_l \|\nabla F(\theta_0)\|^2 + \mathcal{O}(\eta_g^2 \eta_l^2 L \sigma_{orth}^2), \tag{53}$$

where $\sigma_{orth}^2 \leq \sigma_{rand}^2$, leading to faster initial convergence compared to random initialization.

Proof. Using the L-smoothness assumption and the variance bound from Lemma 4, the descent lemma gives:

$$F(\theta_1) \le F(\theta_0) - \eta \|\nabla F(\theta_0)\|^2 + \frac{L\eta^2}{2} \mathbb{E}[\|\Delta W\|^2].$$
 (54)

Substituting the variance bounds $\sigma_{\rm orth}^2 \leq \sigma_{\rm rand}^2$ completes the proof. \Box

Theorem 8 (Stability Against Client Drift). The orthogonal initialization reduces the client drift in the first T rounds by a factor of $\mathcal{O}(1/\kappa(Q))$, where $\kappa(Q)=1$ is the condition number of the orthogonal matrix Q.

Proof. Let $W_k^{(t)}$ be the local parameters of client k at round t. The client drift can be bounded as:

$$\sum_{k=1}^{S} \|W_k^{(t)} - W^{(t)}\|_F \le \sum_{k=1}^{S} \|W_k^{(0)} - W^{(0)}\|_F + \text{gradient divergence terms.}$$
(55)

Under orthogonal initialization, $||W_k^{(0)} - W^{(0)}||_F = 0$ for all k in the relevant subspace, significantly reducing the initial drift compared to random initialization where this term can be substantial.

Lemma 6 (Preservation of Pre-trained Features). The base weight construction $W_{base} = W_0 - Q[:, 1:r_s]R[1:r_s,:]$ preserves the pre-trained model's representation capacity while making room for task-specific adaptations.

Proof. The modification subtracts only the principal components corresponding to the top- r_s singular vectors, which typically capture the most redundant or adaptable features. The remaining weight matrix $W_{\rm base}$ retains the bulk of the pre-trained knowledge while being orthogonal to the adaptation subspace.

Corollary 3 (Compatibility with Federated Aggregation). *The orthogonal initialization ensures that the QR-based aggregation operates on well-conditioned matrices, improving numerical stability and convergence properties.*

Proof. Since all client parameters are initialized within the same orthonormal basis, the concatenated matrix $B_{\text{concatenated}}$ has orthogonal columns, ensuring that the QR decomposition in the aggregation step is numerically stable and preserves the subspace structure effectively.

Theorem 9 (Initialization Stability). Under L-smoothness of each F_k and the orthogonal initialization scheme, the expected loss after the first communication round satisfies:

$$\mathbb{E}[F(W_1)] \le F(W_0) - \eta_g \eta_l \|\nabla F(W_0)\|^2 + \frac{L}{2} \eta_g^2 \eta_l^2 \sigma^2,$$
(56)

and the effective variance term σ^2 is reduced by at least a factor of K compared to random initialization.

Table 15. Comparison of initialization methods for federated LoRA	Table 15. Com	parison of	initialization	methods for	or federated LoRA
---	---------------	------------	----------------	-------------	-------------------

Method	Subspace Consistency	Initial Variance	Drift Resistance	Feature Preservation
Random Gaussian	Х	High	Х	✓
Xavier Uniform	X	Medium	X	✓
Kaiming Normal	X	Medium	X	✓
Orthogonal (ILoRA)	✓	Low	✓	✓

Proof. The result follows from combining the subspace alignment (Lemma 3), variance reduction (Lemma 4), and spectral stability (Lemma 5) properties of orthogonal initialization within the standard federated optimization framework.

Remark 3. The orthogonal initialization in ILoRA provides unique benefits for federated learning:

- Eliminates Initial Misalignment: All clients start in the same subspace, preventing random orientation noise
- Reduces Early-Stage Variance: Concentrates updates in principal directions, reducing gradient variance by O(1/K)
- Accelerates Convergence: More coherent aggregation from the first round enables faster convergence
- **Preserves Pre-trained Knowledge**: Maintains the original model's capabilities while enabling adaptation
- Enhances Numerical Stability: Well-conditioned matrices improve aggregation stability
- Reduces Client Drift: Consistent initialization minimizes early-round divergence

These advantages are particularly crucial in federated settings where system and data heterogeneity exacerbate training instability. The orthogonal initialization establishes a solid foundation for the subsequent QR-based aggregation and control variate mechanisms to operate effectively.

Corollary 4 (Robustness to Rank Heterogeneity). The orthogonal initialization remains effective under rank heterogeneity, as all client subspaces are nested within the global subspace colspan(Q), ensuring compatibility regardless of local rank choices.

Proof. For any client rank $r_k \leq r_s$, the initialization $B_k^{(0)} = Q[:,1:r_k]$ guarantees $\operatorname{colspan}(B_k^{(0)}) \subseteq \operatorname{colspan}(Q)$, maintaining subspace consistency across different rank configurations.

B.4. Control Variates in Rank-Heterogeneous Settings

The integration of control variates with AdamW optimization in rank-heterogeneous federated learning requires careful theoretical treatment. We establish the theoretical foundations and convergence properties of this mechanism, extending classical variance-reduction methods to heterogeneous low-rank subspaces.

Theorem 10 (Convergence with Control Variates and AdamW). Under Assumptions 1-7, with local learning rate η_l and global learning rate η_g satisfying $\eta_l L \leq 1$, the ILoRA framework with control variates and AdamW optimization achieves the convergence rate:

$$\frac{1}{T} \sum_{t=1}^{T} \mathbb{E}[\|\nabla F(\theta_t)\|^2] \leq \mathcal{O}\left(\frac{1}{\sqrt{SKT}} + \frac{\delta^2}{T} + \frac{\sigma^2}{T} + \frac{(r_s - \bar{r})^2}{r_s^2}\right), \tag{57}$$

where the δ^2 term captures the residual client drift after control variate correction, and $(r_s - \bar{r})^2$ represents the rank misalignment error.

Proof. The proof extends the AdamW convergence analysis by incorporating the control variate correction:

Step 1: Moment Update with Correction. The first moment update becomes:

$$m_k^{(t,i)} = \beta_1 m_k^{(t,i-1)} + (1 - \beta_1)(g_k^{\text{raw}} + c^{(t-1)} - c_k).$$
 (58)

Step 2: Bias Analysis. The control variate introduces a bias term bounded by the gradient heterogeneity δ :

$$\|\mathbb{E}[\tilde{g}_k] - \nabla F(\theta)\| \le \|\mathbb{E}[g_k^{\text{raw}}] - \nabla F_k(\theta)\| + \|c^{(t-1)} - c_k - (\nabla F(\theta) - \nabla F_k(\theta))\|.$$

$$(59)$$

Step 3: Variance Reduction. The control variate reduces the effective variance from σ^2 to $\sigma^2(1-\rho^2)$, where ρ is the correlation between local and global gradients:

$$Var(\tilde{g}_k) = Var(g_k^{\text{raw}}) + Var(c^{(t-1)} - c_k) + 2Cov(g_k^{\text{raw}}, c^{(t-1)} - c_k).$$
(60)

Step 4: Rank Misalignment Bound. The projection error due to rank heterogeneity is bounded by:

$$||P_s c^{(t)} - c^{(t)}||^2 \le \mathcal{O}\left((r_s - \bar{r})^2 ||c_k^{(t)}||^2\right).$$
 (61)

Step 5: Combined Analysis. Incorporating these effects into the AdamW convergence proof yields the stated rate.

Theorem 11 (Compatibility with Heterogeneous Ranks). The control variate mechanism in ILoRA remains effective under rank heterogeneity, as the gradient corrections operate within the aligned subspaces established by QR-based aggregation.

Proof. Let $\theta_k \in \mathbb{R}^{d_k}$ denote the parameters of client k with local rank r_k , where $d_k = r_k(d+k)$. The control variate

correction:

$$\tilde{g}_k = g_k^{\text{raw}} + (c^{(t-1)} - c_k)$$
 (62)

operates entirely within the client's local parameter space. Since the QR-based aggregation ensures that all client subspaces are aligned with the global subspace $\operatorname{colspan}(Q)$, the correction terms $c^{(t-1)}$ and c_k can be consistently represented and applied across different ranks.

Lemma 7 (Bias-Variance Tradeoff). The control variate correction in ILoRA reduces the variance of local updates while introducing negligible bias under moderate data heterogeneity.

Proof. The variance reduction follows from:

$$Var(\tilde{g}_k) = Var(g_k^{raw}) + Var(c^{(t-1)} - c_k) + 2Cov(g_k^{raw}, c^{(t-1)} - c_k).$$
(63)

When $c^{(t-1)} \approx \nabla F(\theta)$ and $c_k \approx \nabla F_k(\theta)$, the covariance term becomes negative, reducing the overall variance. The bias is bounded by:

$$\|\mathbb{E}[\tilde{g}_k] - \nabla F(\theta)\| \le \|\mathbb{E}[g_k^{\text{raw}}] - \nabla F_k(\theta)\| + \|c^{(t-1)} - c_k - (\nabla F(\theta) - \nabla F_k(\theta))\|.$$
(64)

Lemma 8 (Variance Reduction via Control Variates). *Under Assumptions 4-6, the variance of the corrected gradient is reduced relative to the raw gradient:*

$$\mathbb{E}\|\tilde{g}_k^{(t)} - \nabla F(\theta_t)\|^2 \le (1-\rho) \,\mathbb{E}\|\nabla F_k(\theta_t) - \nabla F(\theta_t)\|^2 + \rho \,\sigma^2,\tag{65}$$

where $0 < \rho < 1$ depends on the update frequency of c_k and the learning rates η_l, η_q .

Proof. The control variate correction effectively reduces the component of gradient noise that is correlated with the difference between local and global control states. The parameter $\rho \in (0,1)$ acts as a variance decay factor that quantifies the effectiveness of the control variate correction, controlled by the synchronization interval and learning rate configuration. When control variates are well-synchronized, ρ approaches 1, indicating perfect variance reduction.

Lemma 9 (Rank-Aligned Aggregation Error Bound). Let r_k and r_s be the local and server-side ranks, respectively. Then the projection of control states onto the global subspace obeys:

$$||P_{s}c^{(t)} - c^{(t)}||^{2} \leq \sum_{k \in S_{t}} p_{k}^{2} ||(P_{s} - P_{k})c_{k}^{(t)}||^{2}$$

$$\leq \mathcal{O}\left((r_{s} - \bar{r})^{2} ||c_{k}^{(t)}||^{2}\right),$$
(66)

where \bar{r} is the mean client rank.

Proof. The bound follows from the subspace containment property (Assumption 4) and the fact that the projection error scales with the squared difference between server and

client ranks. When all r_k are close to r_s , the mismatch-induced aggregation error is second-order small. \Box

Proposition 3 (Adaptation to Non-IID Data). The control variate mechanism in ILoRA automatically adapts to the degree of data heterogeneity, providing stronger correction under high non-IID settings.

Proof. The control variate difference $c^{(t-1)} - c_k$ approximates $\nabla F(\theta) - \nabla F_k(\theta)$, which grows with increasing data heterogeneity. This provides a self-adjusting correction mechanism that becomes more aggressive as client drift increases, effectively adapting to the local data distribution without requiring explicit hyperparameter tuning.

Lemma 10 (Communication Efficiency of Control Variates). The control variate mechanism in ILoRA adds minimal communication overhead, requiring only $O(\max_k d_k)$ additional parameters per client, where d_k is the dimension of client k's local parameters.

Proof. Each client transmits $\Delta c_k \in \mathbb{R}^{d_k}$ in addition to its model parameters. Since $d_k = r_k(d+k) \ll d \times k$ (the dimension of the full weight matrix), the overhead is negligible compared to the model parameters:

$$\frac{C_{\text{control}}}{C_{\text{model}}} = \frac{r_k(d+k)}{dk} = \mathcal{O}\left(\frac{r_k}{\min(d,k)}\right) \ll 1.$$
 (67)

Since $r_k \ll \min(d, k)$ in low-rank adaptation, this ratio is typically less than 1%.

Theorem 12 (Stability Under Rank Changes). The control variate mechanism in ILoRA maintains stability even when clients dynamically change their LoRA ranks, provided the rank changes are within the global subspace colspan(Q).

Proof. When a client changes its rank from r_k to r'_k , its parameter space dimension changes from d_k to d'_k . However, since both subspaces are contained within $\operatorname{colspan}(Q)$, the control variates can be projected between these subspaces using the orthogonal basis Q, preserving the correction effectiveness. The control state c_k can be appropriately truncated or zero-padded to match the new dimension while maintaining its directional information.

Corollary 5 (Generalization Improvement). The control variate mechanism in ILoRA improves generalization by reducing overfitting to local data distributions while maintaining adaptation capacity.

Proof. By correcting local gradients toward the global direction, the control variates prevent clients from overoptimizing for their local distributions, thereby improving generalization to unseen data from the global distribution. This regularization effect emerges naturally from the bias-variance tradeoff inherent in the control variate correction.

Table 16. Comparison of drift mitigation methods in federated LoRA

Method	Rank Heterogeneity	AdamW Compatibility	Comm. Overhead	Theoretical Guarantees
FedProx	✓	Х	Low	Partial
SCAFFOLD	X	X	Medium	Strong
FedCM	✓	✓	Medium	Partial
ILoRA Control	✓	✓	Low	Strong

Algorithm 3 Rank-Heterogeneous ILoRA Control Variate Update

- 1: Client k (round t):
- 2: Receive global control $c^{(t-1)}$ and parameters $\theta^{(t-1)}$
- 3: Compute raw gradient: $g_k^{\mathrm{raw}} \leftarrow \nabla_{\theta} F_k(\theta_k)$ 4: Apply correction: $\tilde{g}_k \leftarrow g_k^{\mathrm{raw}} + (c^{(t-1)} c_k)$
- 5: Apply AdamW optimizer: $\theta_k \leftarrow \text{AdamW}(\theta_k, \tilde{g}_k; \eta)$
- 6: Compute control delta: $\Delta c_k \leftarrow g_k^{\text{raw}} c_k$
- 7: Update local control: $c_k \leftarrow g_k^{\text{raw}}$
- 8: Send $(\theta_k, \Delta c_k)$ to server
- 9: **Server:**
- 10: Aggregate control deltas: $\Delta c \leftarrow \frac{1}{S} \sum_{k \in S_t} \Delta c_k$ 11: Update global control: $c^{(t)} \leftarrow c^{(t-1)} + \Delta c$
- 12: Broadcast $c^{(t)}$ to clients

Remark 4. The control variate mechanism in ILoRA provides several unique advantages:

- Rank-Agnostic Operation: Works seamlessly with heterogeneous client ranks through subspace alignment
- AdamW Integration: Naturally combines with adaptive optimization without compromising convergence guaran-
- Adaptive Correction: Self-adjusts based on data heterogeneity, providing stronger correction under high non-IID settings
- Minimal Overhead: Adds negligible communication cost while providing significant convergence improvements
- Theoretical Guarantees: Provides provable convergence under non-IID data and rank heterogeneity
- Dynamic Adaptation: Maintains stability under client rank changes through subspace projection
- Generalization Enhancement: Improves model generalization by reducing local overfitting

These advantages make the control variate mechanism particularly suitable for practical federated learning scenarios where system heterogeneity, data heterogeneity, and resource constraints are common challenges.

Corollary 6 (Robustness to System Heterogeneity). The control variate mechanism in ILoRA maintains effectiveness under system heterogeneity, as the correction operates independently of client-specific computational capabilities and communication patterns.

Proof. The control variate correction depends only on the

Table 17. Communication cost comparison of federated LoRA methods.

Method	Downlink Cost	Uplink Cost	Ranks
FedIT	$\mathcal{O}(r(d+k))$	$\mathcal{O}(S \cdot r(d+k))$	X
FLoRA	$\mathcal{O}(r_{\text{total}}(d+k))$	$\mathcal{O}(r_{\text{total}}(d+k))$	✓
LoRA-FAIR	$\mathcal{O}(r(d+k))$	$\mathcal{O}(S \cdot r(d+k))$	X
FFA-LoRA	$\mathcal{O}(r(d+k))$	$\mathcal{O}(S \cdot r(d+k))$	X
ILoRA	$\mathcal{O}(r_s(d+k))$	$\mathcal{O}(S \cdot r_{\max}(d+k))$	✓

gradient directions and control states, which are invariant to system-level variations such as computation speed, memory capacity, or network latency. This decoupling ensures robustness to the diverse system characteristics typically encountered in federated learning deployments.

B.5. Communication Efficiency Analysis

The communication efficiency of ILoRA stems from its innovative combination of QR-based aggregation, orthogonal initialization, and rank-aware control variates. We provide a comprehensive analysis of the communication costs and compare them with existing federated LoRA methods.

Theorem 13 (Total Communication Cost of ILoRA). The total communication cost per round in ILoRA is bounded

$$C_{ILORA} = \mathcal{O}\left(r_s(d+k) + S \cdot \max_k(r_k(d+k)) + S \cdot \max_k d_k\right), \tag{68}$$

where r_s is the server rank, r_k are client ranks, $d \times k$ is the weight matrix dimension, and $d_k = r_k(d+k)$ is the control variate dimension for client k.

Proof. The communication cost decomposes into three components:

1. Server-to-Client Broadcast:

$$C_{\text{downlink}} = \underbrace{r_s(d+k)}_{\text{global model}} \\ + \underbrace{S \cdot \max_k(r_k(d+k))}_{\text{personalized parameters}} \\ + \underbrace{S \cdot \max_k d_k}_{\text{control variates}}$$

$$(69)$$

2. Client-to-Server Upload:

$$C_{\text{uplink}} = \underbrace{S \cdot \max_{k} (r_k(d+k))}_{\text{client updates}} + \underbrace{S \cdot \max_{k} d_k}_{\text{control deltas}}$$
(70)

3. Total per Round:

$$C_{\text{total}} = C_{\text{downlink}} + C_{\text{uplink}} = \mathcal{O}\left(r_s(d+k) + S \cdot \max_k (r_k(d+k)) \right) + S \cdot \max_k d_k$$

Lemma 11 (Comparison with Baseline Methods). Let $r_{\text{max}} = \max_k r_k$ and $r_{total} = \sum_k r_k$. The communication costs of different federated LoRA methods are:

- **FedIT**: $\mathcal{O}(S \cdot r(d+k))$ (homogeneous ranks only)
- FLoRA: $\mathcal{O}(r_{total}(d+k))$
- LoRA-FAIR/FFA-LoRA: $O(S \cdot r(d+k))$ (homogeneous ranks only)
- ILoRA: $\mathcal{O}(r_s(d+k) + S \cdot r_{\max}(d+k))$

Proof. The costs are derived as follows:

- **FedIT**: Assumes homogeneous rank r, broadcasts global model to all clients. - **FLoRA**: concatenateds all client parameters, cost scales with total rank r_{total} . - **LoRA-FAIR/FFA-LoRA**: Homogeneous rank methods, similar to FedIT. - **ILoRA**: Server maintains rank r_s , clients use personalized ranks $r_k \le r_s$.

Proposition 4 (Scalability Advantage). *ILoRA achieves* better scalability than FLoRA as the number of clients S increases, with the communication cost ratio:

$$\frac{C_{ILoRA}}{C_{FLoRA}} = \mathcal{O}\left(\frac{r_s}{r_{total}}\right) = \mathcal{O}\left(\frac{1}{S}\right) \quad \text{when } r_k = \Theta(1).$$
(72)

Proof. When client ranks are bounded $(r_k = \Theta(1))$, we have $r_{\text{total}} = \Theta(S)$ while $r_s = \Theta(1)$. Thus:

$$\frac{C_{\rm ILORA}}{C_{\rm FLORA}} = \frac{\mathcal{O}(r_s(d+k))}{\mathcal{O}(r_{\rm total}(d+k))} = \mathcal{O}\left(\frac{1}{S}\right). \tag{73}$$

Theorem 14 (Optimality of QR Compression). The QR-based aggregation in ILoRA achieves the information-theoretic minimum communication cost for preserving the column space of the aggregated client updates.

Proof. Let $\Delta W = \sum_{k=1}^S p_k B_k A_k$ be the exact aggregated update. The QR decomposition $\Delta W = QR$ with rank- r_s truncation preserves the principal column space while using only $r_s(d+k)$ parameters. Any further compression would

necessarily lose information about the column space, making this representation optimal for subspace preservation according to the Eckart-Young theorem.

Lemma 12 (Control Variate Overhead Analysis). *The communication overhead from control variates in ILoRA is negligible compared to the model parameters:*

$$\frac{C_{control}}{C_{model}} = \mathcal{O}\left(\frac{\max_k r_k}{\min(d, k)}\right) \ll 1. \tag{74}$$

Proof. The control variate dimension is $d_k = r_k(d + k)$, while the full model dimension is $d \times k$. Thus:

$$\frac{C_{\text{control}}}{C_{\text{model}}} = \frac{r_k(d+k)}{dk} = \mathcal{O}\left(\frac{r_k}{\min(d,k)}\right). \tag{75}$$

Since $r_k \ll \min(d, k)$ in low-rank adaptation, this ratio is typically less than 1%.

Proposition 5 (Bandwidth-Delay Product Optimization). *ILoRA optimizes the bandwidth-delay product by reducing the number of communication rounds through improved convergence stability, while maintaining low per-round communication cost.*

Proof. The orthogonal initialization and control variates reduce client drift, leading to faster convergence (fewer rounds T). The total communication volume is:

$$V_{\text{total}} = T \cdot C_{\text{per-round}}.$$
 (76)

ILoRA reduces both T (through stability improvements) and $C_{\text{per-round}}$ (through QR compression), providing multiplicative savings in the bandwidth-delay product.

Theorem 15 (Trade-off between Communication and Accuracy). For a fixed total communication budget B, ILoRA achieves better accuracy than FLoRA by optimally allocating the budget between communication rounds and perround precision.

Proof. Let $B=T\cdot C$ be the total budget, where T is rounds and C is cost per round. ILoRA allows more rounds $(T_{\text{ILoRA}}>T_{\text{FLoRA}})$ due to lower C, while maintaining comparable per-round precision through QR aggregation. This leads to:

$$Accuracy_{ILoRA}(B) > Accuracy_{FLoRA}(B)$$
 (77)

for the same total budget B, as more communication rounds generally lead to better model convergence. \Box

Corollary 7 (Energy Efficiency). *ILoRA reduces the energy consumption of federated training by decreasing both communication time and computational requirements per round.*

Proof. The energy consumption is proportional to:

$$E \propto T \cdot (E_{\text{comm}} + E_{\text{comp}}).$$
 (78)

Table 18. Summary of ILoRA's end-to-end performance guarantees

Performance Aspect	Theoretical Guarantee	Practical Benefit
Convergence Rate	$\mathcal{O}(1/\sqrt{SKT})$ with heterogeneity terms	Fast model training even with non-IID data and system diversity
Communication Cost	$\mathcal{O}(r_s(d+k) + S \cdot r_{\max}(d+k))$	Scalable to thousands of clients with minimal overhead
Rank Heterogeneity	Exact aggregation for arbitrary $r_k \le r_s$	Clients can choose ranks based on local resources
Training Stability	Drift reduction by $\mathcal{O}(1/\kappa(Q))$	Reliable convergence without oscillation or divergence
Non-IID Robustness	Adaptive control variate correction	Automatic handling of diverse data distributions
Real-World Deployment	Theoretical guarantees preserved under constraints	Practical usability in resource-limited environments

ILoRA reduces T (fewer rounds), E_{comm} (less data transfer), and E_{comp} (smaller local models and more efficient aggregation), providing comprehensive energy savings.

Algorithm 4 Communication-Efficient Protocol in ILoRA

- 1: Initialization:
- 2: Server computes $Q, R \leftarrow QR(W_0)$ and sets W_{base}
- 3: Server initializes all clients with orthogonal slices B_{r_k}, A_{r_k}
- 4: Each Communication Round:
- 5: Clients compute local updates and control deltas
- 6: Clients upload: $(B_k, A_k, \Delta c_k)$ total: $\mathcal{O}(r_k(d+k))$
- 7: Server aggregates via QR: $\Delta W \leftarrow B_{\text{concatenated}} A_{\text{concatenated}}$
- 8: Server computes: $Q, R \leftarrow QR(\Delta W)$
- 9: Server personalizes: $B_{r_k} \leftarrow Q[:, 1:r_k], A_{r_k} \leftarrow R[1:r_k]$
- 10: Server broadcasts: (B_{r_k}, A_{r_k}, c) total: $\mathcal{O}(r_s(d+k))$

Remark 5. The communication efficiency of ILoRA provides several practical advantages:

- Scalability: Supports large-scale deployments with many clients through $\mathcal{O}(\log S)$ scaling
- Resource Adaptation: Accommodates clients with different computational capabilities through rank heterogeneity
- **Network Friendly**: Reduces bandwidth requirements for constrained environments
- Cost Effective: Lowers operational costs for cloud-based federated learning
- Energy Efficient: Reduces both communication and computation energy consumption
- Theoretically Optimal: Achieves near-optimal communication for subspace preservation
- Practical Deployment: Compatible with real-world network constraints and client diversity

These advantages make ILoRA particularly suitable for practical federated learning deployments where communication efficiency is a critical concern.

Corollary 8 (Real-World Applicability). *ILoRA's communication efficiency enables practical deployment in resource-constrained environments including mobile devices, edge computing systems, and bandwidth-limited networks, while maintaining theoretical performance guarantees.*

Proof. The combination of low-rank adaptation (reducing parameter count by $O(r_k/\min(d,k))$), QR-based compression (achieving optimal subspace preservation), and minimal control variate overhead (less than 1% additional communication) ensures that ILoRA maintains practical communication requirements. This enables deployment under severe resource constraints while preserving the convergence and stability guarantees established in Theorems 5-10.

Theorem 16 (Comprehensive Performance Guarantee of ILoRA). *Under the theoretical framework established in Sections B.1-B.5, ILoRA simultaneously achieves the following performance guarantees:*

- 1. Convergence Guarantee: $\mathcal{O}\left(\frac{1}{\sqrt{SKT}} + \frac{\delta^2}{T} + \frac{(r_{\max} r_s)^2}{T}\right)$ convergence rate under heterogeneous data and rank settings.
- 2. **Training Stability**: Client drift reduction by factor $\mathcal{O}(1/\kappa(Q))$ with $\kappa(Q) = 1$, and gradient variance reduction by $\mathcal{O}(1/K)$
- 3. Communication Efficiency: $\mathcal{O}(\log S)$ scaling with client population and $\mathcal{O}(r_s \cdot \max(d, k))$ per-round cost
- 4. Rank Heterogeneity Robustness: Exact aggregation and subspace consistency for arbitrary client ranks $r_k \leq r_s$

5. Non-IID Adaptation: Automatic adjustment to data heterogeneity through control variates

Proof. The comprehensive performance guarantee follows from the synergistic integration of ILoRA's core mechanisms:

- Convergence follows from Theorem 5 and Theorem 10, combining QR aggregation, orthogonal initialization, and control variates
- **Stability** is ensured by orthogonal initialization (Theorem 8) reducing initial misalignment and control variates (Theorem 11) mitigating client drift
- Communication efficiency derives from QR compression optimality (Theorem 14) and scalability advantage (Proposition 4)
- Rank robustness is guaranteed by exact reconstruction (Lemma 1) and subspace preservation (Theorem 6)
- **Non-IID adaptation** emerges from the control variate mechanism's self-adjusting correction (Proposition 3)

The individual guarantees combine multiplicatively rather than additively, as each mechanism addresses distinct challenges while complementing others. For instance, orthogonal initialization enhances QR aggregation stability, which in turn improves control variate effectiveness, creating a virtuous cycle of performance improvements.

Remark 6 (Practical Implications). The comprehensive guarantees in Theorem 16 have significant practical implications:

- **Deployment Flexibility**: ILoRA can be deployed across diverse environments from data centers to edge devices
- **Resource Adaptation**: Automatic adaptation to varying client capabilities through rank heterogeneity
- **Performance Predictability**: Theoretical guarantees provide confidence in real-world performance
- **Scalability**: Logarithmic scaling enables large-scale federated learning deployments
- **Robustness**: Resilience to system heterogeneity, data heterogeneity, and network constraints

These properties make ILoRA particularly suitable for practical federated learning scenarios where theoretical guarantees must translate to real-world performance.

B.6. Summary of Theoretical Guarantees

ILoRA's integrated design provides comprehensive theoretical guarantees, including: provable convergence under data and rank heterogeneity; client-independent communication efficiency; exact aggregation for arbitrary ranks; training stability through subspace alignment; adaptive non-IID robustness; and practical deployability. Table 18 summarizes these guarantees, establishing ILoRA as a principled framework that addresses all three key challenges while maintaining efficiency.